Relationship between depth and age in the North Pacific Ocean

J. K. Hillier and A. B. Watts
Department of Earth Science, University of Oxford, Oxford, UK

Received 25 August 2004; revised 22 November 2004; accepted 6 December 2004; published 24 February 2005.

[1] The North Pacific contains active mid-oceanic ridges and the oldest, Jurassic (166.8 ± 4 Ma), drilled oceanic crust. Its bathymetry is therefore critical to studies of the applicability of thermal contraction models (e.g., the infinite half-space and cooling plate) to the subsidence of seafloor with crustal age. The bathymetry, however, contains seamounts and oceanic islands (e.g., Mid-Pacific Mountains), oceanic plateaus (e.g., Hess, Magellan, and Shatsky), and midplate topographic swells (e.g., Hawaii), which are unrelated to the current plate-scale thermal state of the oceanic lithosphere. We use here a regional-residual separation algorithm called MiMIC to remove these features and to isolate the depths associated with the subsidence of North Pacific oceanic crust. These depths, z (m), increase with time, t (Ma), as $z = 3010 + 307\sqrt{t}$ until 85 Ma. For greater ages the depths ''flatten'' and asymptotically approach ~6.1 km and are well described by $z = 6120 - 3010 \exp(-0.026t)$. The flattening is not ''abrupt'' as recently described in z-t curves produced using the mean, median, and mode. As a result, the depths of both young and old seafloor are fit well (mean difference between and observed and calculated depths of 75 ± 54 m 1σ) by a single cooling plate model. Using a thermal conductivity, k, of 3.138 mW m^{-2} as previous studies, however, gives a plate of similar thickness (i.e., thermal thickness, L, of ~115 km) but one which is unreasonably hot (i.e., temperature at the base of the plate, T_b, of 1522 °C) and inexpansive (i.e., coefficient of thermal expansion, α, of 2.57×10^{-5} °C^{-1}). More reasonable values (i.e., $T_b = 1363$°C, $k = 3.371$ W m^{-1} °C^{-1}, $\alpha = 2.77\times10^{-5}$ °C^{-1}, and $L = 120$ km) are obtained if the crustal thickness is used to constrain T_b and a certain amount of the surface heat flow is allowed to be radiogenically generated within the oceanic lithosphere.

Citation: Hillier, J. K., and A. B. Watts (2005), Relationship between depth and age in the North Pacific Ocean, *J. Geophys. Res.*, *110*, B02405, doi:10.1029/2004JB003406.

1. Introduction

[2] The oceanic crust increases in depth, or subsides, as it ages [e.g., *Menard and Smith*, 1966; *Vogt*, 1967]. The North Pacific contains active mid-oceanic ridges and the oldest drilled, Jurassic age (167 ± 4 Ma) [*Castillo et al.*, 1992; *Floyd and Castillo*, 1992; *Pringle*, 1992], crust. As a result, North Pacific bathymetry is critical to studies investigating the applicability of thermal contraction-type models [*Langseth et al.*, 1966; *McKenzie*, 1967] to the subsidence. Models advocated include the cooling half-space [*Davis and Lister*, 1974; *Davies and Pribac*, 1993], cooling plate [*Parsons and Sclater*, 1977; *Stein and Stein*, 1992; *Johnson and Carlson*, 1992], and CHABLIS [*Doin and Fleitout*, 1996]. Irrespective of the model however, the parameters involved are determined by fitting a theoretical depth-age curve to empirical depth-age data believed to best represent the basin-wide thermal state of the lithosphere.

0148-0227/05/2004JB003406$09.00

[3] The North Pacific seafloor, however, also contains bathymetric features at ''small'' (i.e., seamounts and oceanic islands) and ''medium'' (i.e., oceanic plateaus and isolated ''hot spot swells'' [e.g., *McNutt and Fischer*, 1987; *Sichoix et al.*, 1998]) scales compared to the large, or ''plate-scale,'' increase in depth with age (Figure 1). These features, which dominantly occur on old (>80 Ma) seafloor in the western Pacific, appear to be superimposed on the plate-scale bathymetry, and their current topographic expressions are therefore unrelated, we assume, to the thermal contraction of the cooling models.

[4] Early methods for isolating the plate-scale bathymetry were intuitive. *Menard* [1969, p. 276] used the ''best known and least complicated localities'' to show a ~3200 m depth difference between the ridge crest and the deep ocean basins. *Sclater et al.* [1971] carefully selected more depths representative of ''normal'' seafloor where magnetic anomalies could be picked along bathymetric profiles (up to 16 depth estimates per chron). This showed the first ''clear'' depth-age relationship for the oceans up to crustal ages of 80 Ma. *Parsons and Sclater* [1977] added similar data to this curve for crust >80 Ma, and this combined

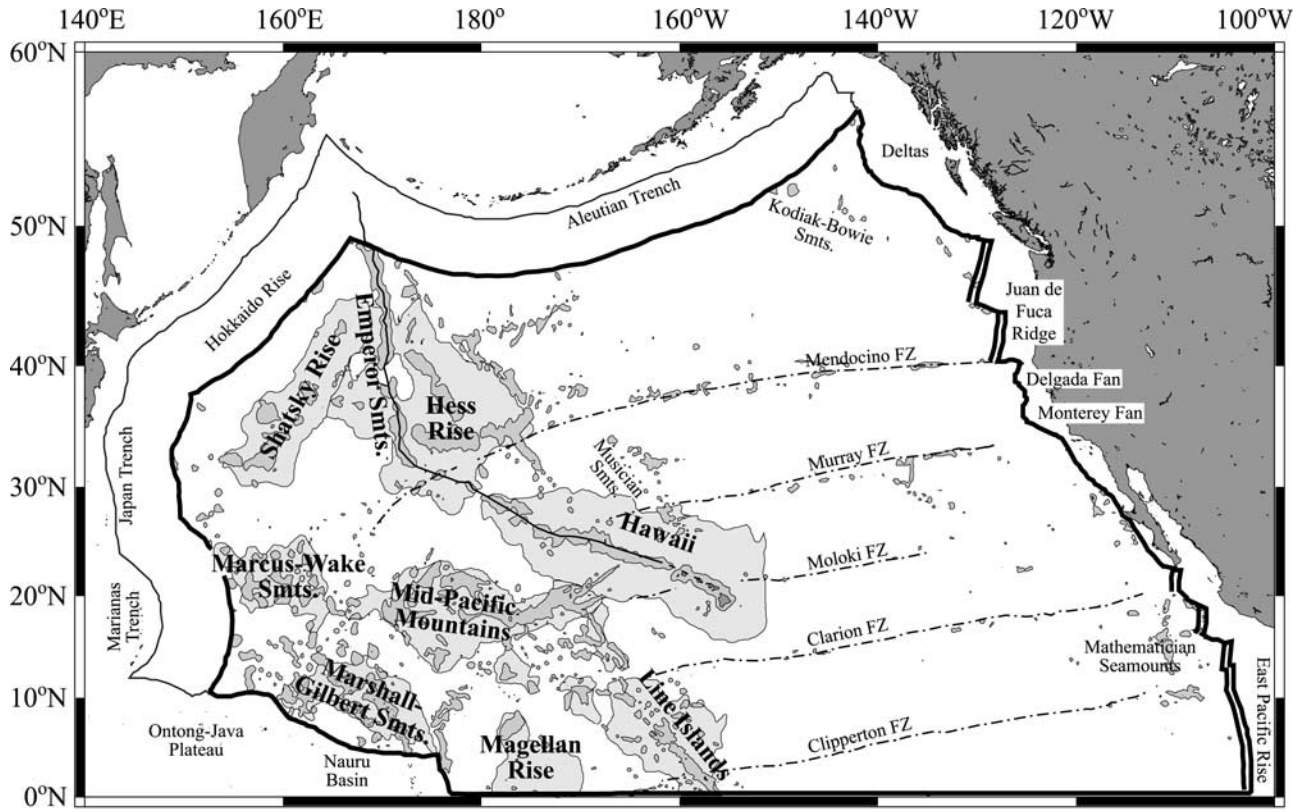

Figure 1. North Pacific. Dark gray shading is small-scale features such as seamounts based on the 500 m contour of the smoothed (50 km median) data from Figure 5a. Light gray shading is medium-scale features from Figure 5b. The area analyzed, surrounded by a bold outline, contains only the data that best represent the plate-scale subsidence of the seafloor (see text). Double parallel lines indicate active spreading. Fracture zones (FZ) are approximately located.

data set is shown as solid circles joined by a bold solid line on Figure 2. The disadvantage of these data sets is that they only contain small amounts of data.

[5] *Schroeder* [1984] followed the work of *Heestand and Crough* [1981] in the North Atlantic and constructed a $1° \times 1°$ "grid" of arithmetic means of ship track data. The grid was then used to remove the effect of "hot spots" [e.g., *Crough*, 1978] by excluding $1° \times 1°$ values within a preferred distance, i.e., 800 km (distances 0 to 1800 km investigated), of a hot spot or its track. The remaining values were isostatically corrected for loading by sediments using data of *Crough* [1983] and the sediment thickness compilation of *Ludwig and Houtz* [1979]. *Schroeder* [1984, p. 9876] "used the presence of seamounts is used as a criterion for hot spot recognition," and so, we believe that seamounts and oceanic plateaus were excluded as well as hot spot swells. The flexural bulges seaward of the trenches were accounted for by excluding all bathymetric data within 400 km of the trench axes. The thick dashed line on Figure 2 shows the best fit curve of *Schroeder* [1984]. However, because Schroeder's technique degrades the data from old seafloor, *Schroeder* [1984, p. 9873] found it "impossible to distinguish between the infinite half-space and cooling plate models of the lithosphere using the age-depth data in the Pacific Ocean."

[6] *Renkin and Sclater* [1988] also reassessed the earlier studies as they believed them to be "not complete" because of the limited amount of the depth-age data used. They used the SYNBAPS [*Van Wykhouse*, 1973] compilation of ship track bathymetry data. They correct for sedimentary loading like *Schroeder* [1984], but in contrast, they estimate the depth to the top of representative mid-ocean ridge generated basement by using a modal technique. In this technique, data are placed in 100 m by 1 Myr bins and a contour containing approximately two thirds of the data computed, a recomputation of which is shown as the dark gray shading on Figure 2. However, in areas where unperturbed seafloor (shown in white in Figure 1) is rare, common depth modal averaging may underestimate regional depths [see *Hillier and Watts*, 2004]. On the other hand, the technique of *Renkin and Sclater* [1988] does not exclude depth data, so estimates for all ages are possible. Nevertheless, *Renkin and Sclater* [1988] considered their database "too limited" to construct an empirical depth-age curve.

[7] *Marty and Cazenave* [1989] used the DBDB-5 (SYNBAPS II) data set and corrected for sediment loading by using the empirical relation determined by *Schroeder* [1984]. *Marty and Cazenave*'s [1989, p. 302] analysis consists of two stages, taking a $2° \times 2°$ mean to "eliminate short wavelength topographic signals" then iteratively fitting a linear $z = A + B\sqrt{t}$ regression line, where z is depth in km and t is time in Ma, and excluding data $>$ $\pm$1000 m away from it. According to this analysis, oceanic depth almost everywhere appears to increase linearly with

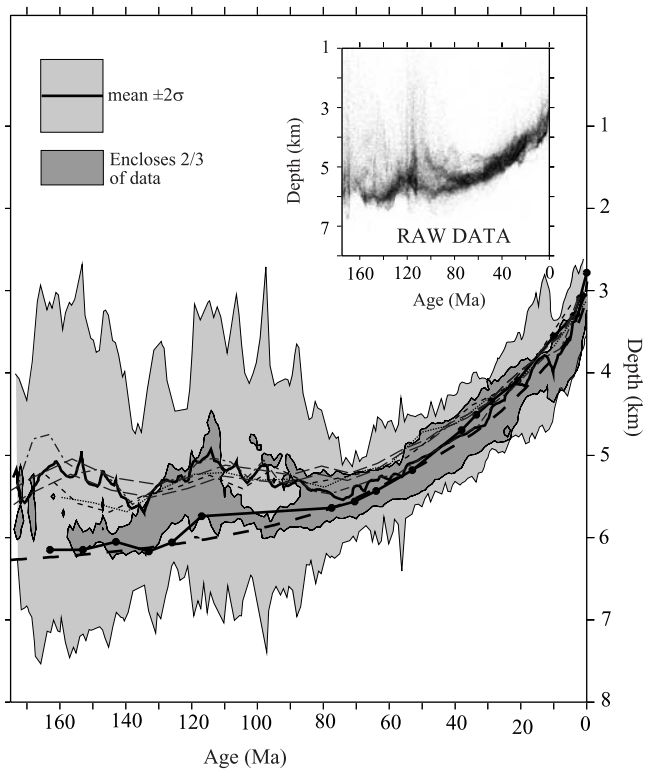

Figure 2. Depth versus age plot of previous estimates of regional depth in the North Pacific. Thick dashed line is empirical fit (square root then exponential) of *Schroeder* [1984] for the North Pacific. Data of *Sclater et al.* [1971], extended to >80 Ma by *Parsons and Sclater* [1977] for the North Pacific are shown as dots joined by a thick solid line. Other bold line is mean over every 1 Myr of the SYNBAPS data compilation [*Renkin and Sclater*, 1988] (all qualities of sediment data) with 2σ (standard deviations) shown as light gray. Thinner lines are examples of determinations using other statistical estimators: 5 Myr mean of DBDB-5 from *Stein and Stein* [1993, Figure 7] (dash-dotted), North Pacific; 10 Ma mode with age of ship track data and ETOPO-5 from *Morgan and Smith* [1992, Figure 2] (short-dashed and dots, respectively), whole Pacific; and median with time of a regional (400 km) spatial median of North Pacific ship tracks with and without sediment unloading correction (two long-dashed lines) [*Smith*, 1990; *Stein and Stein*, 1993]. Note the similarity between curves produced using these statistical estimators. Dark gray shading is the most common depths outlined by a contour that encloses approximately two thirds of the ship track data [*NGDC*, 2003a] points after *Renkin and Sclater* [1988]. Bins are 100 m by 1 Myr. Inset shows the raw data, in this case the modes of ship track data from the NGDC catalogue [*NGDC*, 2003a] taken over 0.1° × 0.1° (blockmode of GMT [*Wessel and Smith*, 1998]).

the square root of crustal age. However, means incorporate outliers and thus do not exclude the bias toward shallow depths due to seamounts, some of which remains after the second stage because features which rise up to 2000 m above the ridge-generated basement may not be removed (>2000 m if any normal basement is removed). With this bias dominantly on old seafloor, zero-age seafloor depth is overestimated (i.e., too deep), and the subsidence rate is underestimated. Consequently, the bias also causes the age at which data appear to be consistent with subsidence as the square root of age to be erroneously extended.

[8] *Colin and Fleitout* [1990] use a sediment-corrected SYNBAPS bathymetry and a method similar to that of *Marty and Cazenave* [1989] but with $z = A + B\sqrt{t} + Ct^2$. The extra t^2 term makes an assessment of any preconceived bias due to the form of their chosen *z-t* relation difficult. The features that rise above the normal seafloor, however, are still present. Thus we suspect some biases also remain. On the other hand, we note that C is always negative, and so *Colin and Fleitout* [1990] are able to strongly state that the seafloor flattens beyond the square root of time subsidence at old ages.

[9] *Stein and Stein* [1993, p. 60] assert that "The choice of data used to derive the model is crucial." In particular, they argue against the exclusion of data because the exclusions increase the influence of a priori assumptions on the process being modeled. They fit cooling plate model GDH1 to DBDB-5 bathymetry averaged (i.e., mean) in every 2 Myr interval, which expressly includes seamounts, isolated hot spot swells, and oceanic plateaus (see thin dash-dotted line Figure 2). If one adopts the cooling plate model, however, the exclusion of some data is implicitly necessary. For example, the cooling plate model does not model crustal thickness variations (e.g., at seamounts), so the exclusion of seamounts from the data to be fitted by the model introduces no assumptions beyond those made in adopting the cooling plate model. Indeed, the exclusion is, we believe, necessary. The raw DBDB-5 bathymetry used by *Stein and Stein* [1992, 1993], sediment corrected or otherwise, is therefore not suitable for comparison with theoretical cooling plate model curves. Since curves for the regional (400 km) median-filtered [*Smith*, 1990] depths and the same depths after sediment correction [*Stein and Stein*, 1993] and the modal depths of ETOPO-5 [*National Oceanic and Atmospheric Administration* (*NOAA*), 1988] and ship track data [*Morgan and Smith*, 1992] all appear similar (thin lines on Figure 2), the same criticism may also apply to them. These curves are all considerably (∼500 m) shallower for $t > 80$ Ma than the earlier data sets of *Parsons and Sclater* [1977] and *Schroeder* [1984].

[10] In summary, depth-age curves based on analysis of recent gridded data using statistical estimators (i.e., mean, median, mode) are consistently shallower than earlier more empirical (i.e., generated by a principally intuitively process rather than by a numerical technique) curves such as those of *Parsons and Sclater* [1977] and *Schroeder* [1984]. The difference becomes large at an "abrupt" [*Carlson and Johnson*, 1994; *Smith and Sandwell*, 1997] flattening of the recent curves at ∼70 Ma such that no cooling plate model can adequately explain the subsidence of both young and old seafloor [*Carlson and Johnson*, 1994]. Thus, while debate exists about the shape of the depth-age curve representing the plate-scale thermal state of the North Pacific oceanic lithosphere, the best thermal boundary layer model to describe the subsidence, if any can, also remains uncertain.

[11] In this paper we attempt to determine the depth-age curve representative of the plate-scale thermal state of the

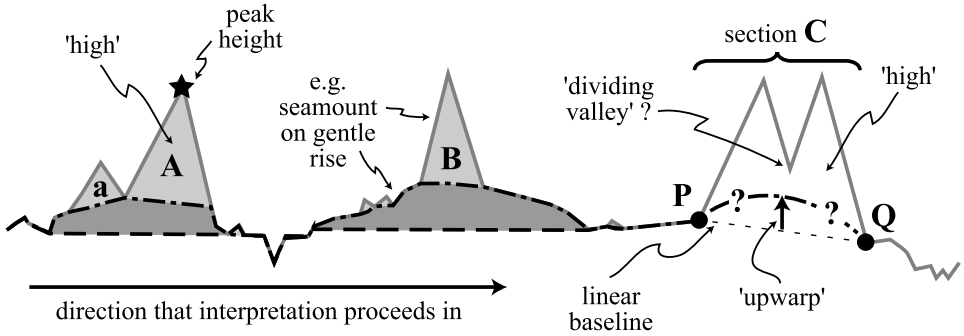

Figure 3. Illustration of the operation of MiMIC [*Hillier and Watts*, 2004] on a schematic bathymetric profile. See text for description. Solid dark gray line is bathymetry. Left of point P, dashed line is "regional" bathymetry (without small-scale bathymetric highs) deduced when the morphology of highs is not considered. Dot-dashed line is same but when morphology of highs is required to be "seamount-like" (i.e., for MiMIC set parameters $\bar{z}$, ϕ, and $\mathcal{U}$). Gray shadings (dark and light combined) are the highs "found" in the former case; light grays only (e.g., A, B, and a) are those found in the latter. A and a illustrate effect of restricting permissible peak height locations to center of sections (parameter ϕ). B is a seamount on a gentle rise and illustrates effect of restricting permissible range of $\bar{z}$. Section C illustrates $\mathcal{U}$, a quantification of the dilemma as to whether it is better to continue the interpretation directly between P and Q or to make the central dip a dividing valley.

North Pacific oceanic lithosphere by applying a regional-residual separation algorithm, called MiMIC [*Hillier and Watts*, 2004], to the bathymetry of the North Pacific. MiMIC approximates the intuitive style of analysis of the early investigators, applies this to modern data compilations, and, we believe, separates the plate-scale subsidence from smaller-scale superimposed trends in a simple and reproducible way. The subsidence is then used to determine the "best fit" thermal boundary layer models and thereby estimate values for the main physical parameters of the lithosphere.

2. Analytical Method

[12] MiMIC [*Hillier and Watts*, 2004] is an algorithm for the separation of bathymetry into "regional" and "residual" [e.g., *Wessel*, 1998], namely, relatively large- and small-scale, components. In contrast to previous techniques [e.g., *Smith*, 1990], MiMIC does not find the regional bathymetry directly. Instead, it identifies small-scale bathymetric highs of a specified morphology and removes them to reveal larger-scale trends beneath. The advantages of this are that the morphology of the highs is preserved, they can be accurately assigned to appropriate bathymetric components, and the method is effective even when normal seafloor is rare. Furthermore, oceanic plateaus and hot spot swells are removed without the requirement for an a priori cooling plate reference model, and data are not decimated, thus avoiding problems such as those encountered by *Schroeder* [1984].

[13] MiMIC operates along profiles where it identifies small-scale bathymetric highs in a manner similar to the manual identification of a regional seafloor depths (Figure 3). In interpreting the profile manually (from left to right) we scan ahead of our already estimated regional (dot-dashed line up to point P) considering the highs (e.g., A and B, light gray shading) that it is possible to form, and from these select the high of the most geologically reasonable morphology.

[14] MiMIC systematizes this selection in a two-tier logical loop. The lower level loop searches, up to a maximum distance S_r, for the next point deeper than P, e.g., Q, the section between which is obviously a high. Whenever the lower level loop finds a high, the higher level loop then uses three user-defined morphological parameters (skew ϕ, mean height $\bar{z}$, up-warp $\mathcal{U}$) to determine whether or not this section represents a geological feature. The ϕ and $\bar{z}$ select against sections with their peak height toward their ends and excess low or high seafloor, respectively; thus a, A, B (light gray) are selected (dot-dashed line) instead of the dark gray shaded area (dashed line). $\mathcal{U}$ quantifies the degree to which it is visually reasonable to up-warp a linear baseline, which is related to seafloor roughness, and determines if section C is best divided into multiple features or not. If no section is found, or the section does not fit the criteria for a single geological feature, P is moved on and the process repeated.

[15] Figure 4 shows examples of the application of MiMIC to bathymetric data acquired along ship tracks in the North Pacific Ocean. The first application is to remove small-scale features from the unfiltered bathymetry, and the second application is to remove medium-scale features that remain after the first pass.

[16] The parameters used in the first application (S_r = 200 km, $\mathcal{U}$ = active, $0.2 < \phi < 0.8$, and $0.23 < \bar{z} < 0.75$) are the same as used by *Hillier and Watts* [2004] in the south central Pacific. Figure 4a shows that these parameters isolate seamounts, oceanic islands, and other small-scale features. For some highs, however, the "true" interpretation is ambiguous. Some highs (below the stars in Figure 4), for example, are seemingly truncated at too shallow a depth because the smaller peaks within the high are individually more "seamount-like" in shape than the whole high. This is most obvious at ~7750 km (solid star in Figure 4a) where the "dividing valley" (see Figure 3) between two peaks is large (approximately half the total height). Some highs are truncated beneath where they

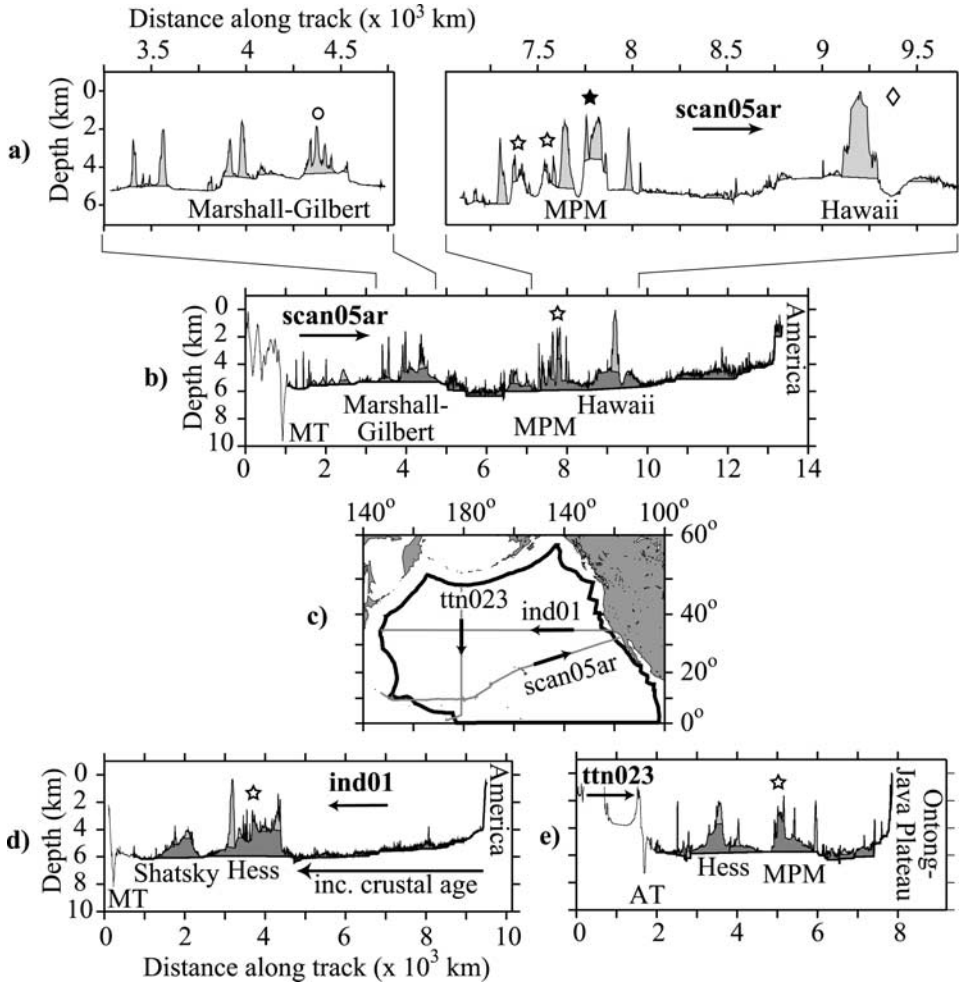

Figure 4. Operation of MiMIC along ship track profiles across the Pacific Basin. (a) Profile showing sections of bathymetry measured during cruise scan05ar. Top line is measured bathymetry, bottom line is bathymetry after the first application of MiMIC, and light gray shading is thus the small-scale bathymetric features isolated by this application. Stars highlight areas where the true interpretation is ambiguous and the regional of MiMIC may appear too shallow. Circle is where regional of MiMIC may be too deep. Diamond is where MiMIC follows seafloor down a flexural moat formed by seamount loading. (c) Map. Gray lines indicate track location, arrows are sailing direction, and bold outline is analysis area as in Figure 1. Cruises are 1976 cruise by research vessel (R/V) *Thomas Washington* NGDC 15040068 (ind01), 1969 cruise by R/V *Argo* NGDC 15010062 (scan05ar), and 1993 cruise by R/V *T. G. Thompson* NGDC 20010022 (ttn023). (b), (d), and (e) Full bathymetric profiles from cruises. Here results of a second application of MiMIC are also shown, and dark gray shading is the medium-scale features isolated. MPM, Mid-Pacific Mountains; MT, Marianas Trench; AT, Aleutian Trench.

arguably should be (below the open circle in Figure 4a). The majority of highs, however, are well isolated.

[17] Since larger features are difficult to collectively parameterize, $\mathcal{U}$, ϕ, and $\bar{z}$ were not set for the second application of MiMIC. After testing, S_r was set to 2000 km. This results in no artificial maximum size constraint being introduced and, specifically, ensures that the Hawaiian Swell is fully isolated. Figures 4b, 4d, and 4e show that MiMIC completely removes the Hawaiian Swell as well as other medium-scale topographic features (e.g., Shatsky and Hess rises).

[18] MiMIC only considers constructional features, so some effects related to the load imposed by volcanic edifices such as flexural moats remain in the bathymetry after its first application. This would lead to a bias toward too deep seafloor, but moats are usually filled with sediment. One notable exception lies to the northeast of the youngest Hawaiian islands, which is well seen at ~9375 km (open diamond, Figure 4a). Ultimately, this makes little difference, however, as the Hawaiian Swell is still well isolated (Figure 4b).

3. Application to the North Pacific

3.1. Data Set

[19] To analyze bathymetry in the North Pacific area, we have applied MiMIC to a gridded data set. We use gridded data because, perhaps surprisingly, they suffer less from

biases due to the spatial distribution of data collected than do simple compilations of the shipboard measurements themselves [*Hillier and Watts*, 2004]. Grids also have the advantage over individual ship tracks in that because tracks intersect, some assessment of errors in the data is possible by crossover analysis [e.g., *Johnson*, 1971; *Wessel and Watts*, 1988; *Wessel*, 1989; *Smith*, 1993]. Errors, for example, may be due to "length unit errors" [*Smith*, 1993] caused by incorrect recording of depth units or "nominal sound velocity" used and "scale errors" [*Smith*, 1993], which arise during the digitization of analogue precision depth recorder traces.

[20] Our analysis is performed, in the first instance, on the predicted bathymetry of *Smith and Sandwell* [1997] once it has been isostatically corrected for sedimentary loading. We use a recent digitization [it *National Geophysics Data Center* (*NGDC*), 2003b] of a compilation of sediment thickness, S, above the "acoustic basement" [*Ludwig and Houtz*, 1979] and a correction, s, of

$$s = 0.224S + 900\left[1 - \exp\left(\frac{-S}{1800}\right)\right] \quad (1)$$

where s and S are in meters [*Schroeder*, 1984].

3.2. Study Area

[21] The area that we investigate is one that we believe contains the depths which best reflect the plate-scale thermal state of the North Pacific oceanic lithosphere. Consequently, the flexural rises within $3\pi/2\lambda$ [*Watts*, 2001] (assuming a broken, semi-infinite plate) of the trenches are excluded from the analysis. The flexural wavelength, λ, is approximately computed from tabulated age, t, versus effective elastic thickness, T_e, estimates [*Watts*, 2001]; $T_e = 6.146\sqrt{t} - 10.817$, with T_e in km and t in Ma. Areas of extensive Cretaceous volcanism in the Ontong-Java Plateau and Nauru Basin and deep-sea sedimentary fans off northwest United States and Canada, where the depth to the top of the unloaded ridge-generated oceanic basement is uncertain, are also excluded from the analysis. The analyzed area is outlined in bold on Figure 1.

[22] Analysis of gridded data with MiMIC uses a mesh of profiles within a rectangular area [*Hillier and Watts*, 2004]. A portion of the mesh is shown inset on Figure 5b. The analysis here, however, is effectively limited to the study area described above by setting depths outside the desired area to sea level.

3.3. Analysis

[23] Figure 5b shows the small-scale features isolated from the gridded bathymetry of *Smith and Sandwell* [1997] (Figure 5a) by a first application of MiMIC. The parameters used are as described for the analysis along

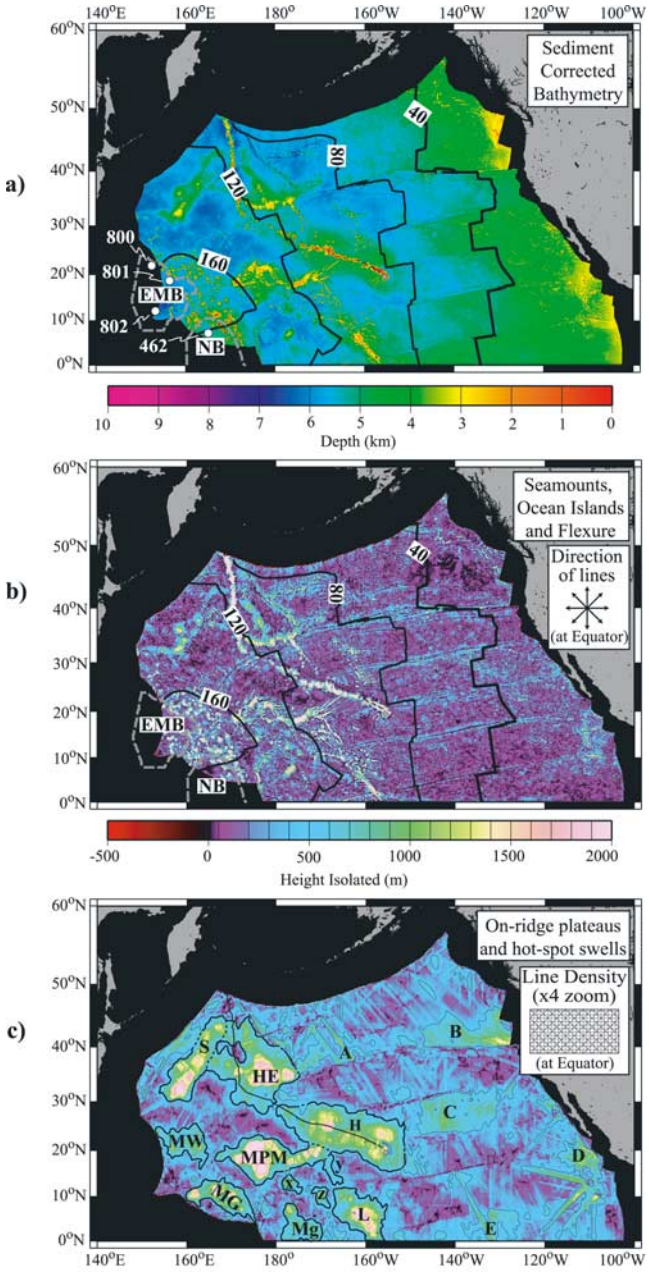

Figure 5. Bathymetric features isolated by MiMIC. (a) Unprocessed bathymetry of the North Pacific from the data set of *Smith and Sandwell* [1997]. Masked areas (black) are those unlikely to contain data reflecting the plate-scale thermal state of the region (see Figure 1 and text). White circles are ODP holes, numbered in white. (b) Small-scale features, i.e., seamounts and oceanic islands, isolated from the unprocessed bathymetry with MiMIC using S_r = 200 km, $\mathcal{U}$ = active, $0.2 < \phi < 0.8$, and $0.23 < \bar{z} < 0.75$. Seafloor ages of *Müller and Roest* [1997] are also shown. NB, Nauru Basin; EMB, East Marianas and Pigafetta basins; see Figure 8. Inset shows the direction of the profile sets used. (c) Medium-scale features, i.e., plateaus, swells, and rises, isolated from bathymetry from which the small-scale features have already been removed, found using no morphological constraints and S_r = 2000 km. Thin line is 500 m contour of data smoothed by a 100 km spatial median filter (i.e., grdfilter [*Wessel and Smith*, 1998]). Bold lines are limits of the features used in the analysis strongly guided by the 500 m contour. S, Shatsky; HE, Hess-Emperor; H, Hawaii; MG, Marshall-Gilbert; MPM, Mid-Pacific Mountains; MW, Marcus-Wake; Mg, Magellan; L, Line Islands. For rest, see text. Inset illustrates the profile density.

profiles shown in Figure 4, but the interpretation based on grids is more stable as each feature is approached from multiple directions. This stability is illustrated if, for example, one considers that a continuous linear ridge will not be detected by a profile along its length but will be detected by a profile crossing it. As a result, by comparison with the initial bathymetry, the small-scale features appear well defined. These features are not related to the plate-scale cooling of the lithosphere. We therefore remove (i.e., subtract) the height isolated in Figure 5b from the initial bathymetry before applying MiMIC again.

[24] The second application of MiMIC also uses parameters as in Figure 4. Figure 5c shows the medium-scale bathymetric highs that have been isolated, and some profile-parallel "noise."

[25] The noise is presumed random and is largely present in the interpretation because insufficient information is known to set $\mathcal{U}$, ϕ, and $\bar{z}$. Therefore, for example, MiMIC does not yet avoid connecting flexural fracture zone troughs. The amplitude of the noise is estimated to be ±250 m because the 500 m isolated height contour (thick and thin solid black lines) is the lowest value contour that is not significantly diverted by obvious noise around anomalies whose shape is better known, e.g., the Hawaiian Swell.

[26] The volume of the medium-scale features is then best estimated as the height displayed, less 250 m, within a manually determined area whose limits are strongly guided by the 500 m contour. These limits are shown on Figure 5c as bold lines and are dashed where they do not exactly follow the 500 m isolated height contour. The medium-scale features unrelated to the plate-scale cooling of the lithosphere can then be removed.

[27] The remainder of this section is a justification of our decisions about whether or not to remove individual features.

[28] Magnetic lineations [*Sager and Han*, 1993; *Nakanishi et al.*, 1999], morphology [*Sager et al.*, 1999], and surface heat flow [*Verzhbitskii and Merklin*, 2000] suggest that the Shatsky Rise, marked S on Figure 5c, formed in the Cretaceous, 135–145 Ma, on or near a mid-ocean ridge. Gravity data support this hypothesis as they indicate that it is in local isostatic equilibrium and therefore a site of over-thickened crust [e.g., *Watts et al.*, 1980; *Sandwell and MacKenzie*, 1989; *Marks and Sandwell*, 1991], predictions in agreement with deep seismic data [*Den et al.*, 1969; *Gettrust et al.*, 1980]. The Shatsky Rise is therefore unrelated to the current thermal state of the lithosphere, and so it is removed.

[29] The Hess Rise is believed to have a similar, but later (~100 Ma), origin on a mid-ocean ridge [*Windom et al.*, 1981; *Vallier et al.*, 1983; *Marks and Sandwell*, 1991; *Clouard and Bonneville*, 2001]. However, the rise is difficult to distinguish from a small-amplitude swell that appears to underlie the Emperor seamount chain. Together, these features are marked HE in Figure 5c. It is unknown whether the rise under the Emperors is supported thermally or compositionally. It is, however, localized and almost certainly related to the mechanism currently active under Hawaii.

[30] The Magellan Rise, marked Mg, is less well studied and is smaller than the other rises, although our determination links it to neighboring small-amplitude rises first noted by *Winterer et al.* [1973]. It formed ~135 Ma (biostratigraphic dating of overlying sediments [*Winterer et al.*, 1973]) on the Magellan microplate (magnetic lineation mapping [*Tamaki and Larson*, 1988]). *Schubert and Sandwell* [1989] and *Larson* [1991], for example, assumed the rise to be in isostatic equilibrium and therefore to have a near- or on-ridge origin similar to the Hess and Shatsky rises. This idea is not contradicted by a low (1.08–1.50 m km^{-1}) ratio of geoid height to topography in the region (see Appendix A1 for details of calculation), since similar values have been reported for other rises (e.g., Hess) [*Sandwell and MacKenzie*, 1989; *Marks and Sandwell*, 1991]. Thus all the oceanic plateaus (S, HE, Mg) are removed from the data used to construct our preferred depth-age curve.

[31] The Line, Marshall-Gilbert, and Marcus-Wake seamounts and the Mid-Pacific Mountains (clusters of small-scale features) appear to be associated with medium-scale bathymetric highs, marked L, MG, MW, and MPM, respectively, on Figure 5c. The correlation is perhaps most clearly seen on Figure 1. The Mid-Pacific Mountains formed in the Cretaceous. Deep Sea Drilling Project (DSDP) data suggest ages of 65–80 and 95–125 Ma [*Rea and Vallier*, 1983], and magnetics and morphology indicate >110 Ma [*Matthews et al.*, 1974; *Winterer and Metzler*, 1984]. Radiometric dates of ~85–100 Ma [*McNutt et al.*, 1990], T_e determinations [*Wolfe and McNutt*, 1991], and morphological indicators [*Heezen et al.*, 1973] imply that the Marcus-Wake seamounts probably originated at a similar time. The Marshall-Gilbert seamounts have two documented volcanic episodes in the Late Cretaceous (~85 Ma) [*Davis et al.*, 1989] and mid-Eocene (~55 Ma) [*Kulp*, 1963]. Any sublithospheric cause (e.g., a thermal plume [*Morgan*, 1971]) for this volcanism is therefore unlikely to still be present. Consequently, the medium-scale depth anomalies associated with the volcanism must be lithospherically supported and unrelated to the current plate-scale thermal state of the lithosphere. By analogy this explanation is also applied to the smaller rises associated with volcanism between the Mid-Pacific Mountains and the Line Islands, marked x, y, z on Figure 5c.

[32] The origin of the Line Islands themselves has been considered more problematic because of their reported association with a gravity high [*Sandwell and Renkin*, 1988]. However, they have a volcanic history similar to that of the Marshall Islands [*Haggerty et al.*, 1982; *Sandwell and Renkin*, 1988], forming in the Cretaceous [e.g., *Jackson and Schlanger*, 1976; *Davis et al.*, 2002] with the most recent eruptions in the mid-Eocene (~38–50 Ma [*Harland et al.*, 1990]) [*Haggerty et al.*, 1982; *Schlanger et al.*, 1984; *Sager and Keating*, 1984], and the gravity high is centered at a longitude of ~150°W (see gravity data of *Smith and Sandwell* [1997]). Thus the gravity high is substantially (~1000 km) east of the Line Islands Rise, which is closely associated with old volcanic edifices. These separations in space and time suggest to us that at present the Line Islands Rise and the gravity high are not directly related. All the volcanism-associated rises (L, MG, MW, MPM, x, y, and z) are therefore removed from our depth-age curve.

[33] The Hawaiian Swell may be "thermal" and isostatically raised by reheating of the lithosphere [*Detrick and Crough*, 1978; *Sandwell and Renkin*, 1988; *Sandwell and MacKenzie*, 1989; *Marks and Sandwell*, 1991], or it may be "dynamically" supported by the upwelling limb of convection within the fluid sublithospheric mantle [e.g., *Watts et al.*, 1985; *Heezen et al.*, 1989; *Moore and Schubert*, 1997].

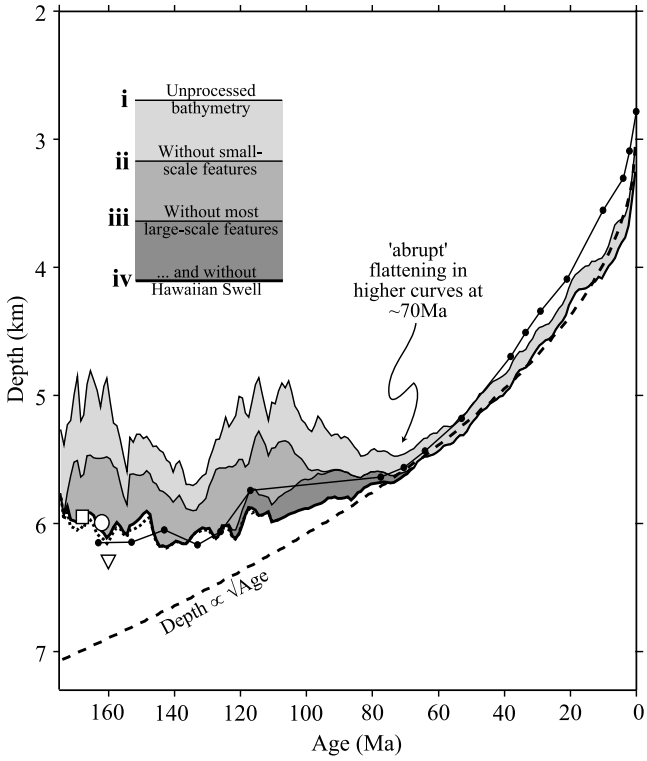

Figure 6. North Pacific depth versus age curves. Curve type i (top) is mean for each 1 Myr of unprocessed bathymetry of *Smith and Sandwell* [1997] (Figure 5a). Curve types ii to iv are progressively deeper because they have small-scale features (Figure 5b) and medium-scale (Figure 5c) rises and plateaus (i.e., not the Hawaiian Swell) and then also have the Hawaiian Swell removed, respectively. Curves iii and iv best reflect the plate-scale thermal state of the Pacific oceanic lithosphere (see text). Note the lack of an abrupt [*Carlson and Johnson*, 1994; *Smith and Sandwell*, 1997] flattening, especially in curve iv. Bottom bold dotted line includes a correction (Figures 8a and 8b) for the effect of Cretaceous volcanism. Joined dots are the data of *Parsons and Sclater* [1977], which are notably similar to curves iii and iv. Ages are from the estimation of *Müller and Roest* [1997] from magnetic lineations. White circle, triangle, and square are loading-corrected basement depth estimates from ODP holes 800, 801 (−5950 m), and 802, respectively (L. Abrams, personal communication, 2004) with ages from magnetic lineations. Estimates at holes 800 and 802 are minimum depths as true basement not reached. Alternative correction for hole 801 based on data from hole 830 gives −6048 m [*Carlson and Johnson*, 1994]. Dashed line is subsidence at a rate that best describes young (<85 Ma) seafloor (see Figures 9a and 9c).

If it is dynamically supported and if the upwelling is locally matched by equal downwelling within the area of the Pacific plate (up and down locally average to approximately zero), then the swell should not be removed. However, if the swell is substantially compensated within the lithosphere or if downwelling occurs in the far-field, e.g., at the trenches, the swell should be removed to best reveal the plate-scale oceanic subsidence. Since we cannot be sure of the origin of the swell, we investigate curves in which it is both retained and removed.

[34] In some areas, marked B and C in Figure 5c, MiMIC isolates highs bounded by fracture zones that are clearly dominantly caused by the age of the oceanic lithosphere. No action is therefore taken to remove these. Similarly, no well-accepted explanation unrelated to plate-scale thermal cooling exists for the highs marked A, D, and E, so they are also not removed.

4. Depth-Age Curves

[35] Figure 6 shows the depth-age curve of the unprocessed bathymetry (curve type i) from the data of *Smith and Sandwell* [1997]. The bathymetry has been assigned ages according to the compilation of *Müller and Roest* [1997]. On young (<50 Ma) seafloor, curve type i of *Smith and Sandwell* [1997] is systematically deeper than the curve of *Parsons and Sclater* [1977]. Since there are no medium-scale features here, this is, we presume, simply because of extra data and more extensive coverage.

[36] Immediately beneath curve i is the curve for the bathymetry after subtraction of the small-scale features (curve type ii). For seafloor younger than ~70 Ma, there is an approximately vertical shift between curves i and ii with a mean offset of 126 ± 10 m (1 standard deviation or 1σ). The effect is greater, 183 ± 16 m (1σ), for older seafloor. In contrast, removal of all the medium-scale features except Hawaii (curve type iii) only affects seafloor >70 Ma, which eliminates the abrupt flattening [*Carlson and Johnson*, 1994; *Smith and Sandwell*, 1997] in the curve at about 70 Ma (Figure 6). This is especially clear in the lowest curve where the Hawaiian Swell has also been removed (curve type iv) shown as a bold line on Figure 6.

[37] Curve iv flattens with increasing seafloor age to a depth of approximately 6 km and correlates well with loading-corrected depths to the top of oceanic basement drilled in Ocean Drilling Program (ODP) holes 801 and 802. It is also the curve that we believe best represents the plate-scale thermal state of the North Pacific oceanic lithosphere.

[38] In general, the curves generated from bathymetries with the medium-scale features removed (curves iii and iv) more closely resemble the curves of *Parsons and Sclater* [1977] and *Schroeder* [1984] than later curves such as those of *Stein and Stein* [1992] and *Morgan and Smith* [1992], which are based on statistical estimators (i.e., the mean, median, or mode) (see Figure 7). We interpret this as indicating that the earlier intuitive selection [*Parsons and Sclater*, 1977] and elimination [*Schroeder*, 1984] techniques, like MiMIC, remove bias toward shallow depths caused by features unrelated to the plate-scale subsidence more effectively than the mean, median, and mode, which have a tendency to pass through topography. In support of this hypothesis we note that on old seafloor (approximately >80 Ma), the curves based on statistical estimators are actually shallower than the majority of the data (computed as by *Renkin and Sclater* [1988]) shown as dark shading on Figure 2.

[39] The variability (2σ) of curve iv for old seafloor (>70 Ma) is 465 m (shown on Figures 9c and 10 in section 5), much reduced from the 1105 m of the unprocessed bathymetry (shown on Figure 2), and gives some idea

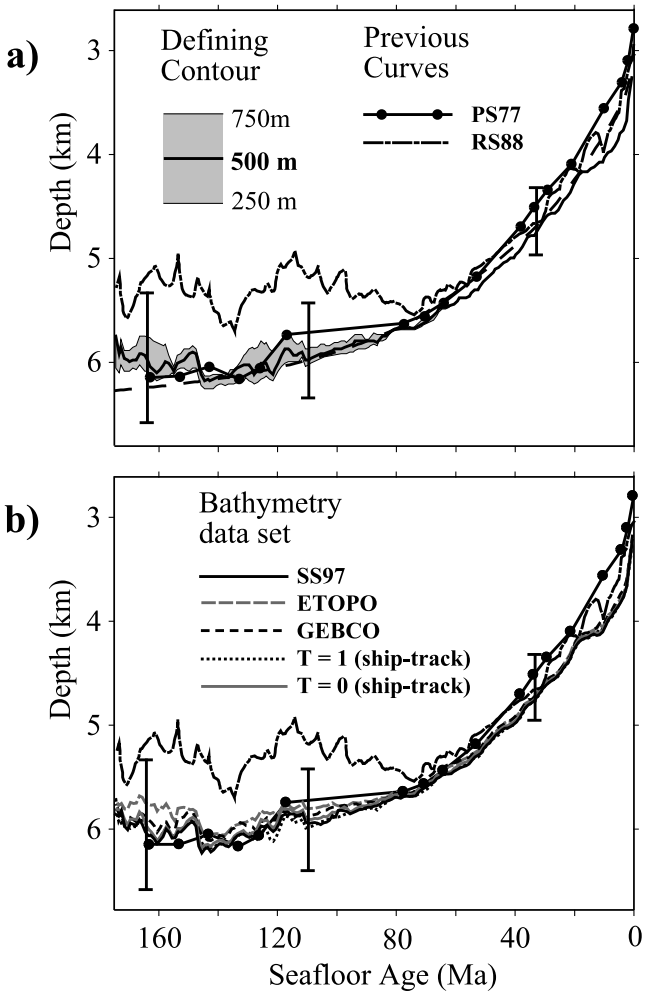

Figure 7. (a) Effect of the contour defining medium-scale features on the depth-age curve. Solid bold line is the mean depths of the bathymetry of *Smith and Sandwell* [1997] after all small- and medium-scale features (Figures 5b and 5c) have been removed using the 500 m contour, curve iv, Figure 6. Gray shading between curves is generated using limits strongly guided by the 250 m (bottom) and 750 m (top) contours. Illustrative error bars are 2σ about mean of bold line. For comparison, bold dots joined by solid line is the depth-age curve of *Parsons and Sclater* [1977], and dot-dashed line is the 1 Myr average of the SYNBAPS data compilation from *Renkin and Sclater* [1988]. All previous depth-age curves are shown on Figure 2. (b) Effect of the bathymetry used on our depth-age curves. Solid bold line is as on Figure 7a. Legend is key for our analyses of available data sets. Curves of *Parsons and Sclater* [1977] and *Renkin and Sclater* [1988] are again shown for comparison.

of the precision of the result. However, systematic factors could affect the accuracy.

4.1. Effect of the Defining Contour

[40] The contour chosen to define the medium-scale features, for example, will influence the result. To evaluate this, Figure 7a shows the variation (gray shading) caused by using 250 m (deeper curve) and 750 m contours (shallower curve), instead of 500 m (bold line), when calculating a curve from which all the medium-scale features are removed (i.e., curve type iv). The data set considered is still that of *Smith and Sandwell* [1997]. For seafloor older than 70 Ma the effect (difference between 250 m curve and 750 m curve) is quite small, 172 ± 97 m (1σ) and does not significantly alter the shape of the curve.

4.2. Effect of the Data Set Used

[41] Figure 7b illustrates the uncertainty associated with the choice of data compilation on curves of type iv (i.e., small-scale and selected medium-scale features removed). The solid line that is computed from the predicted bathymetry of *Smith and Sandwell* [1997], also shown on Figure 6. Equivalent curves computed from ETOPO-5 [NOAA, 1988] and GEBCO [*Intergovernmental Oceanographic Commission (IOC)*, 2003] agree well, differing on average by 100.8 and 70.5 m, respectively. Grids created from spatially binned (i.e., 0.1° × 0.1° blockmode [*Wessel and Smith*, 1998]) ship track data, based on the NGDC compilation, by using splines in tension [*Smith and Wessel*, 1990] ($T = 0$ and $T = 1$) produce depth-age curves that are even more similar to that from the predicted bathymetry. They differ by 21 and 36 m, respectively. The close agreement probably reflects the relatively complete data coverage at the hundreds of kilometers scale in all the data sets.

4.3. Effect of Cretaceous Volcanism

[42] Figure 6 shows that curve iv of the bathymetry of *Smith and Sandwell* [1997] has a slight tendency to become shallower again for ages >140 Ma. Although some return flow models [i.e., *Morgan and Smith*, 1992] predict such an upturn, no rigorous assessment of this can be made. This is due to the difficulty of using seismic reflection profile data to estimate the true top of ridge-generated basaltic basement in the oldest parts of the western Pacific. Here, widespread Cretaceous volcanism [e.g., *Schlanger et al.*, 1981; *Rea and Vallier*, 1983] complicates identification of the depth to the top of true basement.

[43] The western Pacific is characterized on seismic reflection profile data by a so-called "reverberant layer" [*Houtz and Ludwig*, 1979, p. 152], previously called the "lower opaque layer" or "horizon B" [*Ewing et al.*, 1968, p. 3497], below the "smooth acoustic basement" [*Houtz and Ludwig*, 1979]. The layer (a seismic facies) was initially interpreted as being of volcanic or sedimentary origin [*Menard*, 1956; *Winterer et al.*, 1973; *Houtz and Ludwig*, 1979]. *Schroeder*'s [1984] was the first depth-age analysis to isostatically correct seafloor depths for the load of this presumed rock layer using the isopach map of *Houtz and Ludwig* [1979].

[44] Subsequent examinations of seismic reflection and refraction data from studies in the East Marianas Basin [*Shipley et al.*, 1983], however, suggest that a lithological interpretation of this seismically defined layer is "at best tentative" and that the layer is an artifact of the nature of the air gun sound source. Furthermore, drilling at ODP Sites 800–802 shows that the "layer" is better explained by a large impedance contrast across a single lithological boundary [*Lancelot et al.*, 1990].

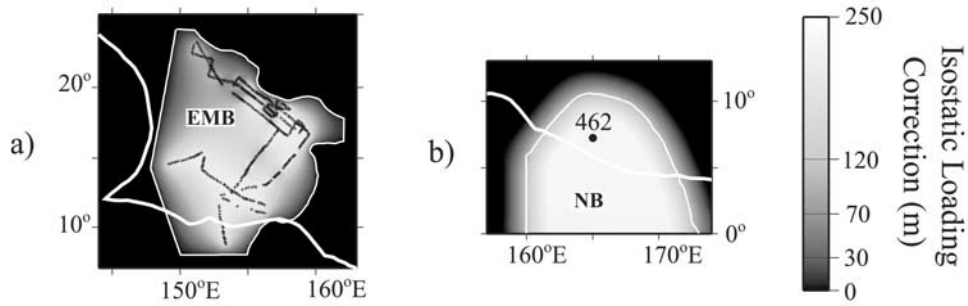

Figure 8. Areas where an isostatic correction for loading of some accuracy is possible for a layer of rock units below the acoustic basement of *Ludwig and Houtz* [1979], yet above the true ridge-generated basaltic oceanic crust for (a) Nauru Basin (NB) and (b) East Marianas and Pigafetta basins (EMB). In the NB, units are Cretaceous volcanic flows, and in the EMB, units are a sediment/sill/flow complex (sediments older than mid-Cretaceous). In the EMB, grid was created by interpolating (i.e., untensioned bicubic spline using surface of GMT [*Wessel and Smith*, 1998]) estimates of layer thickness where there are seismic data (black lines) and forcing values to zero at the edge of the area where there are data (thin white line). In NB, correction is 330 m as described in text but smoothed with a 200 km spatial mean (i.e., grdfilter of GMT [*Wessel and Smith*, 1998]). For location within Pacific, see Figure 5. Thick white line is boundary of study area.

[45] In their analysis of depth-age, *Renkin and Sclater* [1988] considered the new seismic data and assumed up to 0.6 s [*Shipley et al.*, 1983] two-way travel time of material below the acoustic basement of *Ludwig and Houtz* [1979] in the East Mariana Basin. They then isostatically unloaded this material, an effect of about 330 m. *Colin and Fleitout* [1990], however, simply increase depths by 500 m in the area between 160°E–168°W and 9°S–19°N. Since then, further data have become available.

[46] ODP drilling (Site 462), together with seismic data, suggests that the northern Nauru Basin (i.e., north of 6°N) is underlain by a 590–1400 m thick volcanic layer of Cretaceous age [*Shipley et al.*, 1993]. Assuming an unloading correction factor of 0.23 km^{-1} [*Renkin and Sclater*, 1988] and a layer thickness of 1 km, we obtain a basement depth that is deeper than the uncorrected depth by 230 m (Figure 8b). In addition, new seismic data in the East Mariana and Pigafetta basins [*Abrams et al.*, 1993] constrains the thickness of the "sill/flow/sediment lithology" [*Abrams et al.*, 1993] between the acoustic basement and the top of oceanic crust. These data suggest a layer thickness of 400 m and generally on the limit of seismic vertical resolution (~200 m). We have therefore assumed an unloading correction factor of 0.54 km^{-1} [*Renkin and Sclater*, 1988] and a thickness of 400 m where smooth acoustic basement is definitely identified and a thickness of 200 m where it is suspected. The amount this unloading deepens the basement is shown in Figure 8a.

[47] The bold dotted line on Figure 6 shows that correcting for the effect of Cretaceous volcanism has little effect on the depth-age curve produced. However, we caution that constraints on the layer thickness and physical properties remain poor.

4.4. Effect of Seafloor Age

[48] Another uncertainty is seafloor age, especially in the Cretaceous and Jurassic magnetic "quiet zones" [*Renkin and Sclater*, 1988]. We have therefore used the age grid of *Müller and Roest* [1997], which assumes a kinematic model to predict age in the quiet zones. However, these ages are particularly uncertain in the Jurassic because of the lack of drilling constraints [e.g., *Castillo et al.*, 1991; *Müller and Roest*, 1997].

4.5. Possible Effects of Using MiMIC

[49] Finally, we wish to consider the assumption in MiMIC that areas of unusual depth are predominantly highs. The assumption implies that anomalously deep intraplate oceanic areas, for example, deep troughs (e.g., Emperor, Chinook) and under-filled flexural moats, remain in the data while highs are removed. The Emperor and Chinook troughs NE of the Hess Rise only cover, however, a relatively small area of the seafloor. Moreover, the flexural moats of Pacific volcanoes are generally filled, with the notable exception of the southernmost Hawaiian islands. Thus these features will not significantly affect the depth-age curves.

[50] The bathymetric expressions postulated to accompany small-scale (<200 km) "Haxby" [*Wessel et al.*, 1996] gravity lineations [e.g., *Haxby and Weissel*, 1986] are not observed in Figure 5b. This may be because their amplitude is only a few hundred meters [e.g., *Haxby and Weissel*, 1986; *McAdoo and Sandwell*, 1989] and perhaps <50 m (amplitude of best fitting sinusoid across the central Pacific) [*Wessel et al.*, 1996]. The error associated with removing them, if we do so, is therefore small. We also note that similar, but larger-scale, postulated topographic undulations [e.g., *Cazenave et al.*, 1992; *Wessel et al.*, 1996], will, if present, not be removed by our analysis unless they coincide with the medium-scale features that we have previously chosen to remove.

[51] Finally, we acknowledge that some part of the height that we attribute to small-scale features (Figure 5b) could be noise in the data. For example, noise probably accounts for part of the vertical shift between curve i and the other curves in Figure 6. The roughly constant amplitude of the shift on young and least complicated seafloor, however, suggests to

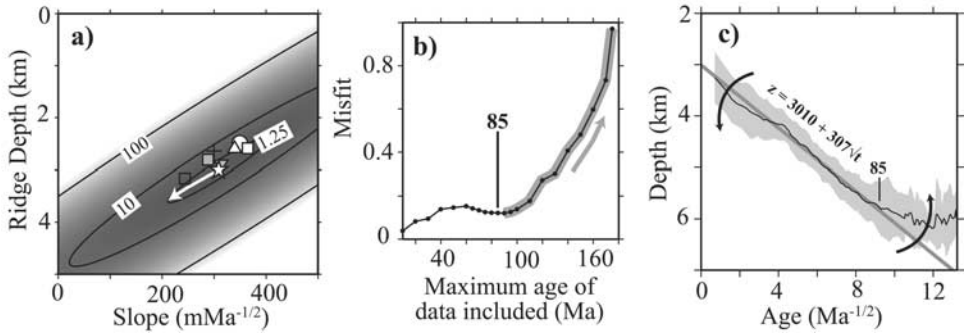

Figure 9. Quantification of rate and extent of subsidence proportional to the square root of crustal age. Data are curve bathymetry of *Smith and Sandwell* [1997] with all small- and medium-scale features removed, curve iv, Figure 6. (a) Misfit ($s^2 = \frac{1}{n}\sum\frac{(z_{\text{model}}-z_n)^2}{\sigma_n^2}$) contour plot for the curves that increase in depth proportional to the square root of age. White star is ridge depth 3010 m, and subsidence rate 307 m Myr$^{-1/2}$ is curve that best fits the data 0–85 Ma. Arrow shows variation of the best fit curve as fit progressively includes data from older seafloor, up to 170 Ma. Other symbols are previous estimates: circle, *Parsons and Sclater* [1977] (North Pacific); open and gray squares, *Marty and Cazenave* [1989] (central North Pacific flow line with ridge depth previously defined and variable, respectively); gray triangle, *Schroeder* [1984] (whole Pacific); white triangle, *Johnson and Carlson* [1992] (global from ODP drill hole data); cross, *Morgan and Smith* [1992] (Pacific); and white square, *Stein and Stein* [1993] (global). Contours are multiples of the minimum misfit. Data are calculated every 1 m Myr$^{-1/2}$, 10 m. (b) Minimum s^2 curves when data from 0 Myr to a fixed limit are inverted for. As data from older seafloor (>85 Ma) are fit, minimum s^2 systematically increases (gray shading and arrow). The 85 Ma age is therefore the oldest seafloor that may be safely described as subsidence proportional to the square root of crustal age. Misfits are calculated using limits at 5 Myr intervals. (c) Best fitting square root of time curve (gray line) to data, shown as mean depths (black line) ±2σ i.e., standard deviation (gray shading). Arrows illustrate the effect of fitting data >85 Ma.

us that the effect of noise is constant across the whole data set. It may therefore affect the zero-age seafloor depth but not the shape of the depth-age curve.

5. Discussion

[52] Young oceanic seafloor subsides at a rate proportional to the square root of crustal age [*Davis and Lister*, 1974; *Parsons and Sclater*, 1977; *Schroeder*, 1984; *Marty and Cazenave*, 1989; *Johnson and Carlson*, 1992; *Stein and Stein*, 1993], which is most easily explained by a so-called [*Vogt*, 1967] "thermal contraction" model [*Langseth et al.*, 1966; *McKenzie*, 1967]. Quantitatively, however, the most appropriate subsidence rate and zero-age depth are still debated (Figure 9a). For the North Pacific, subsidence rates vary from 350 m Myr$^{-1/2}$ [*Parsons and Sclater*, 1977] to 244 m Myr$^{-1/2}$ [*Marty and Cazenave*, 1989], and zero-age depths range from 2500 m [*Parsons and Sclater*, 1977] to 3163 m [*Marty and Cazenave*, 1989]. These ranges increase little when including whole Pacific or global estimates. Also in dispute is the age that the square root of time cooling applies until, which is an important discriminator between thermal contraction models.

5.1. Applicability of the Infinite Half-Space Model

[53] The conductive cooling of an infinite half-space [*Davis and Lister*, 1974] is the simplest thermal contraction model. It predicts that seafloor depth, z, will increase proportionally with the square root of time, t, for seafloor of all ages. Previous, somewhat qualitative, estimates of the age at which oceanic depths become shallower than predicted by the square root of time subsidence, however, range from 20 Ma [*Stein and Stein*, 1993] to rarely deviating at all [*Marty and Cazenave*, 1989]. Intermediate estimates include 55 Ma [*Smith and Sandwell*, 1997], 60–80 Ma [*Parsons and Sclater*, 1977], 80 Ma [*Schroeder*, 1984], and 90 Ma [*Johnson and Carlson*, 1992].

[54] Figure 9a shows the results of an investigation into the fit of the square root of time curves (i.e., $z = A + B\sqrt{t}$) to data between the ages 0 and 85 Ma of curve type iv from the predicted bathymetry [*Smith and Sandwell*, 1997]. A is the zero-age ridge depth (m), and B is the subsidence rate (m Myr$^{-1/2}$). The best fit (white star) is for $z = 3010 + 307\sqrt{t}$. The misfit (contoured on Figure 9a), s^2, between observed (mean over 1 Myr interval) depths, z_n, and model predictions, z_{model}, depths is

$$s^2 = \frac{1}{n}\sum\frac{(z_{\text{model}} - z_n)^2}{\sigma_n^2} \tag{2}$$

where σ_n^2 is the variance of the observations. An age of 85 Ma is chosen because s^2 (bold line on Figure 9b) of the best fitting curve increases systematically when data from seafloor older than this age are included in the inversion, shown by the gray shading and arrow. The 85 Ma age is therefore the oldest age of seafloor that may be safely described as being proportional to the square root of oceanic crustal age. This is a conservative estimate as the systematic increase is only marked from 100 Ma; however, it is robust to the data set used (Table 1). It is greater than the 70 Ma indicated by the curves from which less has been removed

Table 1. Best Fitting Zero-Age Depths and Subsidence Rates for the Range of Crustal Ages Best Described by the Square Root of Time Subsidence[a]

Data Set	Curve	Zero-Age Depth, m	Rate, m Myr$^{1/2}$	Range, Myr
SS97	i	2850^{+140}_{-170}	311^{+27}_{-23}	0–70
SS97	ii	2990^{+170}_{-180}	311^{+29}_{-29}	0–70
SS97	iii	2990^{+170}_{-180}	311^{+29}_{-29}	0–70
SS97	iv	3010^{+170}_{-160}	307^{+27}_{-25}	0–85
ETOPO	iv	2970^{+160}_{-160}	306^{+25}_{-25}	0–85
GEBCO	iv	2970^{+150}_{-130}	305^{+23}_{-21}	0–85
T = 0	iv	3010^{+170}_{-170}	306^{+26}_{-25}	0–90
T = 1	iv	2990^{+180}_{-160}	307^{+28}_{-24}	0–80

[a]SS97 is data of *Smith and Sandwell* [1997], $T = 0$ and $T = 1$ refer to tension used to interpolate ship track data (see section 4.2). Curve indicates which features have been removed; see Figure 6. Errors are estimated from the range of parameter space that is not distinguishable from the minimum misfit with 99% confidence according to the F test [see *Stein and Stein*, 1992], which corresponds to the 1.7 contour on Figure 9a. Age ranges tested at 5 Myr intervals. Note that values are representative of the North Pacific as a whole, but variations within this along "tectonic corridors" probably exist [e.g., *Marty and Cazenave*, 1989; *Kane and Hayes*, 1992].

(SS97 curves i–iii) but still demonstrates a significant deviation from predictions of the infinite half-space model for at least the oldest (100–175 Ma) North Pacific seafloor.

[55] Figure 9c shows that the mean depths of old seafloor (>85 Ma) (black line) deviate from, i.e., become shallower or "flatten" with respect to, the square root of time subsidence that best fits young seafloor (gray line). Here, $t \geq 85$ Ma, measured depths are well (i.e., mean difference 62 ± 54 (1σ) m) approximated by

$$z = 6120 - 3010\exp(-0.026t) \tag{3}$$

On the oldest seafloor (approximately >120 Ma), mean depths are undoubtedly, by greater than 2σ (gray shading), shallower than the square root of time extrapolation from young seafloor. This also appears to be unequivocal on a straight depth-age plot (Figure 6). An explanation for this ~1 km of flattening in the depth-age curve is therefore required.

5.2. Applicability of the Cooling Plate Model

[56] As Figure 9c clearly shows, old (>85 Ma) oceanic seafloor subsides at a rate that smoothly decreases from being proportional to the square root of crustal age, or flattens. Previously suggested mechanisms for the flattening (some originally to explain gravity and heat flow data) include an increase in crustal thickness [*Humler et al.*, 1999], phase changes [*Wood and Yuen*, 1983], a buoyant mantle residuum left over from melt extraction [*Johnson and Carlson*, 1992; *Phipps Morgan et al.*, 1995], dynamic upwelling [*Davies and Pribac*, 1993; *Carlson and Johnson*, 1994] perhaps including internal radiogenic heating [*Jarvis and Peltier*, 1980], return trench-to-axis sublithospheric flow [*Schubert and Turcotte*, 1972; *Schubert et al.*, 1978; *Morgan and Smith*, 1992], thermal rejuvenation of the lithosphere by random hot spot reheating events [*Crough*, 1979; *Heestand and Crough*, 1981; *Nagihara et al.*, 1996; *Smith and Sandwell*, 1997], and generalized thermal input into older lithosphere [*Langseth et al.*, 1966; *McKenzie*, 1967; *Doin and Fleitout*, 1996] perhaps by intense small-scale (λ ~400 km) convection and significant internal heating in the sublithospheric mantle [e.g., *Parsons and McKenzie*, 1978; *O'Connell and Hager*, 1980; *Huang and Zhong*, 2005]. *McNutt* [1995] gives, in our view, an unbiased review of many of these possibilities. However, we limit our analysis to the implications of our empirical depth-age curve for the cooling plate model.

[57] The subsidence, w, of a cooling plate [*Langseth et al.*, 1966] at a given age, t, is described by eight independent parameters [*McKenzie*, 1967]: plate thickness L, plate basal temperature T_b, water temperature T_w, water density ρ_w, coefficient of thermal expansion α, zero-temperature mantle density ρ_0, thermal conductivity k, and heat capacity C_p. Thermal diffusivity κ is equal to $k/\pi\rho_0$ (i.e., density in this relation is assumed independent of temperature) [*Stein and Stein*, 1992]. For comparison to measured depths a zero-age depth, Z_r, is also required. These are related by equations given by *Turcotte and Schubert* [2002] for the subsidence, w,

$$w = \frac{\rho_0\alpha(T_b - T_w)L}{(\rho_0 - \rho_w)}\left[\frac{1}{2} - \frac{4}{\pi^2}\sum_{k=0}^{k=\infty}\frac{1}{(1+2k)^2} \cdot \exp\left(\frac{-(1+2k)^2\pi^2\kappa t}{L^2}\right)\right] \tag{4}$$

and the surface heat flow, q,

$$q = \frac{k(T_b - T_w)}{L}\left[1 + 2\sum_{n=1}^{n=\infty}\exp\left(\frac{-\kappa n^2\pi^2 t}{L^2}\right)\right] \tag{5}$$

Of the nine parameters, T_w, ρ_0, ρ_w, and C_p are assumed to be relatively well known [*Parsons and Sclater*, 1977; *Stein and Stein*, 1992] (Table 2) and Z_r may be deduced from young seafloor (e.g., Figure 9a), which leaves four independent parameters undetermined. The equations describing seafloor subsidence and surface heat flow, however, contain only three independent relationships [*Parsons and Sclater*, 1977], and so only three parameters may be evaluated from

Table 2. Parameters Assumed by *Parsons and Sclater* [1977] and *Stein and Stein* [1992] to be Relatively Well Known

Parameter	Symbol	Value
Water temperature	T_w	0°C
Mantle density (at 0°C)	ρ_0	3330 kg m^{-3}
Water density (at 0°C)	ρ_w	1000 kg m^{-3}
Thermal conductivity	k	3.138 W m^{-1} °C^{-1}
Heat capacity	C_p	1.171 kJ kg^{-1} °C^{-1}

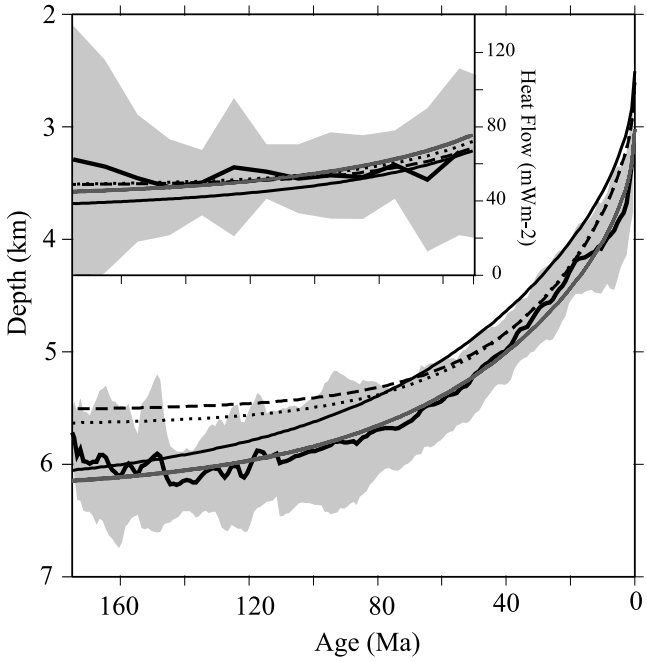

Figure 10. Fit of cooling plate models to depth and heat flow data. Depths (irregular, thick black line) are means for 1 Myr intervals of the bathymetry of *Smith and Sandwell* [1997] after all small- and medium-scale features (Figures 5b and 5c) have been removed using the 500 m contour, curve iv. Gray shading is ±2σ (standard deviations) about the means. Smooth, solid black line is the subsidence of the plate model of *Parsons and Sclater* [1977]. Dotted and dashed lines are the subsidence of global and North Pacific models GDH1 [*Stein and Stein*, 1992] and NPC1 [*Stein and Stein*, 1993]. Gray line is the subsidence of plate models (D, J, K, L–S, T) that best fit these data. Inset (age axis aligned with main plot) is heat flow data [*Pollack et al.*, 1993] of ages >50 Ma [*Stein and Stein*, 1992] used in the inversions. Data (thick black line) are averages for every 10 Myr interval. Gray shading and other lines are heat flow equivalents of the subsidence curves on the main plot.

that data. Since thermal conductivity is comparatively better known [*Parsons and Sclater*, 1977], it is assumed to be 3.138 mW m^{-2}, and the remaining three parameters L, α, and T_b investigated [*Parsons and Sclater*, 1977; *Johnson and Carlson*, 1992; *Stein and Stein*, 1992].

[58] When numerically fitting data, it is necessary to first estimate a zero-age depth [*Stein and Stein*, 1992]. Such a depth is distinct from a ridge depth [*Malinverno*, 1990] in that it does not include axial morphology such as axial horsts [e.g., *Madsen et al.*, 1984; *Wang and Cochran*, 1993; *Buck*, 2001] or median valleys and flank uplifts [e.g., *Sleep and Biehler*, 1970; *Phipps Morgan et al.*, 1987; *Malinverno*, 1990]. To estimate plate parameters for their North Pacific model NPC1, *Stein and Stein* [1993] simply used the same value of 2600 m as for their global model GDH1. We, however, use an estimate from fitting the square root of time curves to young seafloor. Specifically, curve iv of the data set of *Smith and Sandwell* [1997] indicates that 3010 ± 165 m (error from F test; see Table 1) is more appropriate (details in section 5.1). This is similar to previous estimates for the Pacific (shaded symbols on Figure 9a) and agrees well with estimates of 2970–3000 m from other bathymetric data sets (Table 1). However, it is less than one estimate of 3163 m [*Marty and Cazenave*, 1989], which is deeper because this square root of time curve was fitted to data of all ages of data, including older seafloor that is flattening and not best described as a square root of time curve. The arrows on Figures 9a–9c illustrate the effect of including older, flattening seafloor on zero-age depth estimates.

[59] Using the estimated Z_r and keeping T_w, ρ_0, ρ_w, k, and C_p the same as *Parsons and Sclater* [1977] and *Stein and Stein* [1992], the values of the remaining parameters (L, T_b, and α) that fit the data best can then be determined by minimizing the misfit. Misfit, s^2, is

$$s^2 = \frac{1}{n}\sum \frac{(z_{\text{model}} - z_{\text{data}})^2}{\sigma_z^2} + \frac{1}{m}\sum \frac{(q_{\text{model}} - q_{\text{data}})^2}{\sigma_q^2} \qquad (6)$$

where n and m are the number of mean depth and heat flow data, z and q are depth and heat flow, and σ_z and σ_q are standard deviations for the depth and heat flow data [*Stein and Stein*, 1992]. We use a search routine based on a regular mesh of evaluated points across a volume of parameter space and a series of increasing "accuracy levels," which are simply decreasing multiples of the minimum misfit. Initially a broad mesh is used, which contracts until the volume of parameter space within an accuracy contour is well sampled, and then a higher accuracy level is used. This is robust and more efficient than searches with a single resolution mesh.

[60] The search routine for the inversion was tested by assessing its recovery of synthetic curves and reproduction of published results. Parameters used to create theoretical curves are retrieved with accuracies better than 0.2 km, 2°C, and 0.003°C^{-1} for L, Tb, and α, respectively, or ~0.1%. Application of the routine to the data used to deduce GDH1, as tabulated by *Stein and Stein* [1993], gives L = 93.0 km, $\alpha = 3.12 \times 10^{-5}$ °C^{-1} and T_b = 1447°C. These agree with GDH1's parameters (L = 95.0 km, $\alpha = 3.1 \times 10^{-5}$ °C^{-1} and T_b = 1450°C) to within the accuracy (5 km by 25°C by 0.05×10^{-5} °C^{-1}) of their grid search.

5.2.1. Goodness of Fit to Geophysical Data

[61] Figure 10 shows the depths and surface heat flow of the cooling plate model that best fits our processed bathymetry (i.e., curve iv of the data set of *Smith and Sandwell* [1997]) and the (unprocessed) heat flow [*Pollack et al.*, 1993] data from the North Pacific Ocean (see auxiliary material[1]). Curve iv best represents, we believe, the current plate-scale thermal state of the oceanic lithosphere (see section 4), and following *Stein and Stein* [1992], only heat flow from seafloor >50 Ma is used. This model, which we refer to as D (Table 3), uses constants as in studies by *Parsons and Sclater* [1977] and *Stein and Stein* [1992].

[62] The subsidence of this best fit model explains curve iv well, differing from it on average by 75 ± 54 m (1σ). The fit is a significant improvement on either that of *Parsons and Sclater* [1977] (PS77) or (NPC1 and GDH1) of [*Stein*

[1]Auxiliary material is available at ftp://ftp.agu.org/apend/jb/2004JB003406.

Table 3. Parameters for the Best Fitting Cooling Plate Models[a]

			Parameter					Fit		
Model	Data Set	Curve	T_b	α	L	k	Note[b]	z	q	s^2
A	SS97	i	1437^{+191}_{-233}	$2.80^{+0.85}_{-0.47}$	93^{+25}_{-17}	3.138		187.9	4.56	0.399
B	SS97	ii	1468^{+191}_{-200}	$2.69^{+0.64}_{-0.43}$	97^{+19}_{-15}	3.138		117.6	5.03	0.441
C	SS97	iii	1524^{+189}_{-177}	$2.53^{+0.44}_{-0.35}$	116^{+24}_{-16}	3.138		87.1	6.60	0.418
D	SS97	iv	1522^{+184}_{-175}	$2.57^{+0.43}_{-0.36}$	115^{+22}_{-15}	3.138		74.6	6.55	0.414
E	SS97	v	1526^{+165}_{-171}	$2.57^{+0.42}_{-0.31}$	117^{+21}_{-14}	3.138		67.8	6.66	0.377
F	GEBCO	iv	1521^{+191}_{-188}	$2.57^{+0.49}_{-0.36}$	112^{+19}_{-14}	3.138		71.0	6.32	0.458
G	ETOPO	iv	1515^{+194}_{-198}	$2.60^{+0.51}_{-0.36}$	108^{+20}_{-14}	3.138		87.0	6.05	0.464
H	$T = 0$	iv	1528^{+153}_{-172}	$2.55^{+0.41}_{-0.32}$	117^{+24}_{-14}	3.138		74.1	6.64	0.384
I	$T = 1$	iv	1531^{+151}_{-187}	$2.55^{+0.42}_{-0.31}$	116^{+27}_{-16}	3.138		74.9	6.58	0.398
J	SS97	iv	1368^{+6}_{-5}	$2.56^{+0.39}_{-0.30}$	129^{+17}_{-21}	$3.90^{+0.87}_{-0.87}$	1	75.6	6.59	0.414
K	SS97	iv	1363^{+7}_{-7}	$2.57^{+0.42}_{-0.30}$	130^{+23}_{-25}	$3.92^{+0.89}_{-0.84}$	1	74.5	6.59	0.414
L	SS97	iv	1903^{+224}_{-192}	$2.58^{+0.41}_{-0.36}$	92^{+17}_{-12}	2.0		74.7	6.58	0.414
M	SS97	iv	1704^{+203}_{-181}	$2.58^{+0.42}_{-0.35}$	103^{+19}_{-13}	2.5		74.3	6.55	0.414
N	SS97	iv	1557^{+172}_{-183}	$2.58^{+0.40}_{-0.35}$	113^{+23}_{-14}	3		74.7	6.56	0.414
P	SS97	iv	1440^{+175}_{-153}	$2.58^{+0.42}_{-0.35}$	122^{+24}_{-15}	3.5		75.2	6.54	0.414
Q	SS97	iv	1344^{+168}_{-139}	$2.58^{+0.43}_{-0.36}$	130^{+20}_{-16}	4.0		75.0	6.56	0.414
R	SS97	iv	1271^{+155}_{-147}	$2.58^{+0.41}_{-0.36}$	138^{+12}_{-17}	4.5		74.9	6.54	0.414
S	SS97	iv	1212^{+128}_{-112}	$2.56^{+0.44}_{-0.29}$	146^{+4}_{-18}	5.0		75.3	6.56	0.414
T	SS97	iv	1490^{+189}_{-176}	$3.21^{+0.57}_{-0.43}$	104^{+14}_{-12}	3.138	2	73.3	5.61	0.433
U	SS97	i	1398^{+184}_{-220}	$3.36^{+0.44}_{-0.57}$	87^{+19}_{-15}	3.138	2	188.7	5.47	0.363
V	SS97	iv	1409^{+171}_{-162}	$2.77^{+0.47}_{-0.37}$	116^{+22}_{-14}	3.138	3	75.3	6.08	0.390
W	SS97	iv	1487	2.79	112	3.138	4	70.2	6.23	-
X	SS97	iv	1363^{+7}_{-7}	$2.77^{+0.47}_{-0.32}$	120^{+21}_{-21}	$3.37^{+0.86}_{-0.71}$	1, 3	75.5	6.09	0.390

[a]Models are labeled by capital letters and described in the text. Data set is the bathymetry used in the inversion: SS97 is predicted bathymetry of *Smith and Sandwell* [1997], GEBCO is from *IOC* [2003], ETOPO is from *NOAA* [1988], and $T = 0$ and $T = 1$ are grids formed by interpolating ship track data; see section 4.2. Curve indicates curve types i–v described in section 4. Examples for SS97 are on Figure 6. T_b is plate basal temperature (°C), α is the coefficient of thermal expansion ($\times 10^{-5}$ °C^{-1}), L is plate thickness (km), k is thermal conductivity (W m^{-1} °C^{-1}). Errors estimated from the limits of parameter space that is not distinguishable from the minimum misfit with 99% confidence according to the F test, which corresponds to a 1.7 contour on Figure 11a–11c. Error indicates that parameter was inverted for (except model W, see Appendix A). Z_r used for each data set are as in Table 1. Fit is the mean unsigned difference between model and data for depth, z, and heat flow, q. s^2 as in the text.

[b]Notes are 1, crustal thickness constraint used and k inverted for; 2, 4 mW m^{-2} of surface heat flow assumed radiogenic as that of *Parsons and Sclater* [1977]; 3, effect of using different misfit criterion (data as D); and 4, force Z_r to 2600 m as GDH1 [*Stein and Stein*, 1992].

and Stein, 1993]. The fit of our models to the heat flow is also good, differing by 6.55 ± 5.47 mW m^{-2} (1σ). This is better than the mean difference of 9.56 ± 6.59 mW m^{-2} (1σ) of PS77 but worse than 4.51 ± 4.33 and 4.76 ± 4.41 for NPC1 and GDH1, respectively. The worse fit is probably because more weight is effectively given to bathymetry in our inversion because of its much lower variances (variance of curve iv is approximately half of the unprocessed data). Asymptotic depth and surface heat flow for our best fit model are ∼6230 m and ∼41.5 mW m^{-2}, respectively, intermediate between PS77 (6400 m, 34 mW m^{-2}) and GDH1 (5650 m, 48 mW m^{-2}), and in excellent agreement with the best available *z-t* and *q-t* data of *Nagihara et al.* [1996] from basins containing old seafloor in the North Atlantic and North Pacific (e.g., Pigafetta Basin).

[63] The subsidence and surface heat flow data, however, can be equally well produced by cooling plates that have constants and variables different from those of model D. Indeed, 12 models, 7 of which for example have differing fixed values of k (see section 5.2.2), fit the data and overlie each other on the gray line on Figure 10. This occurs because of the number of independent relationships in the z and q equations (see earlier). Namely, inverting *z-t* and *q-t* data for three of the variables α, k, T_b, and L can find a plate that well describes the subsidence largely irrespective of the values of the other constants (i.e., T_w, ρ_0, ρ_w, C_p, and the remaining variable). Equally, for the same reason, one cannot uniquely invert for the four variables simultaneously unless there is some constraint from additional data, crustal thickness for example. Furthermore, investigation of the different bathymetric data sets, models F–I (Table 3), demonstrates similar results to those described above for the data set of *Smith and Sandwell* [1997].

[64] To summarize, in contrast to the conclusions of *Carlson and Johnson* [1994], the bathymetry and heat flow for all ages of seafloor in the North Pacific can, we believe, be approximately described by a single cooling plate model. This is not dependent on the assumed value of k or the bathymetric data set used. It is premature, however, to conclude that the North Pacific oceanic lithosphere behaves as a conductively cooling plate. We first need to assess how physically reasonable the values of the parameters required by the best fit models are.

5.2.2. Consistency With Experimental Determinations of Physical Properties

[65] Model D (Table 3) assumes the same constants (T_w, ρ_0, ρ_w, k, and C_p) and inverts for the same parameters (L, T_b, and α) as *Parsons and Sclater* [1977] and *Stein and Stein* [1992]. Figures 11a–11c show the parameters that best fit curve iv (L = 115 ± 16 km, $\alpha = 2.57 \pm 0.40 \times 10^{-5}$ °C^{-1}, and T_b = 1522 ± 180°C), indicated by a white star. With best fits spanning the ranges L = 108–117 km, $\alpha = 2.55$–2.60×10^{-5} °C^{-1}, and T_b = 1515–1531 °C, the other bathymetric data sets agree well (models F–I, Table 3).

[66] These best fitting models therefore imply a very hot relatively inexpansive plate of intermediate thickness. Most uncontroversial of these properties is the plate thickness of approximately 115 km. This is intermediate between previous global [*Johnson and Carlson*, 1992;

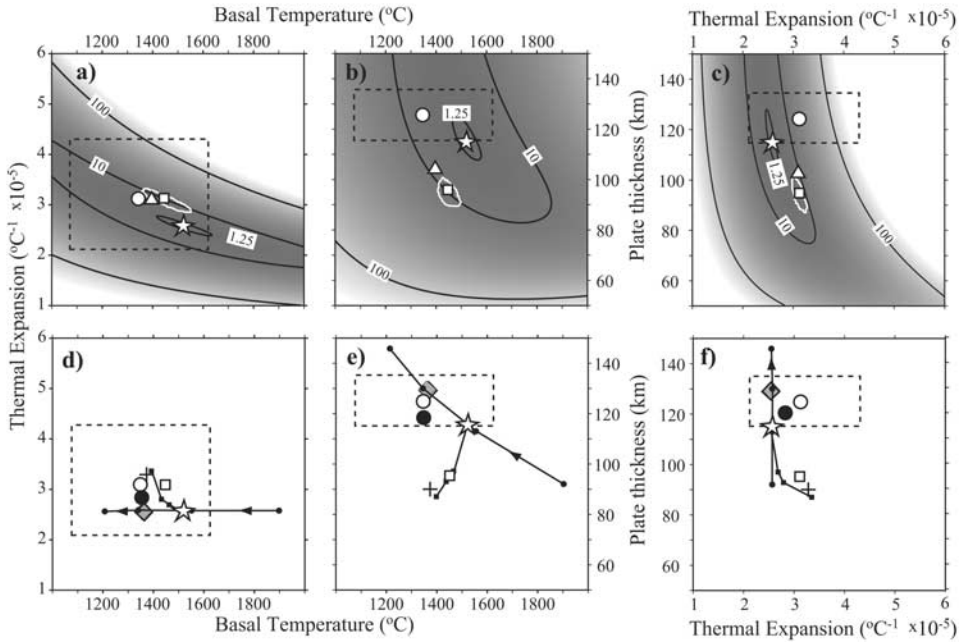

Figure 11. Parameters of best fitting plate models. (a)–(c) A single inversion with constants (T_w, ρ_0, ρ_w, k, and C_p) and variable parameters (L, T_b, and α) same as *Parsons and Sclater* [1977] and *Stein and Stein* [1992] but fit to data in Figure 10. This is model D. Z_r is 3010 m (Figure 9a). Best fit is a white star at L = 115 ± 16 km, α = 2.57 ± 0.40 × 10^{-5} °C^{-1}, and T_b = 1522 ± 180°C. Other symbols are previous estimates: white circle and dashed error box, *Parsons and Sclater* [1977]; white square and white ×1.25 misfit error ellipse, *Stein and Stein* [1993]; and triangle, *Johnson and Carlson* [1992]. Shading (calculated every 5°C, 0.05 × 10^{-5} °C^{-1}, and 1 km) and contours are multiples of the minimum misfit. Figures 11a and 11c show the previously observed inverse relationships that occur because the depths for young and old ages depend on the products of α T_b and $\alpha T_b L$, respectively [*Stein and Stein*, 1992]. (d)–(f) Illustration of the effect of two trends: (1) effect of progressively including bathymetric features then forcing a 2600 m [*Stein and Stein*, 1992] ridge depth (models E, D, C, B, A, then U) (shown as line with black squares moving away from star; cross is North Pacific model NPC1 [*Stein and Stein*, 1993]) and (2) effect of increasing k (models L to S). Line with black circles (arrow indicates direction of increase). Also shown is effect of constraining inversion with crustal thickness, shown as gray diamond (model K) largely hiding open diamond (model J). Black circle is parameters of model X, our preferred values.

Stein and Stein, 1992] and Pacific [*Parsons and Sclater*, 1977; *Stein and Stein*, 1993] estimates.

[67] More notable, however, is the basal temperature of about 1520°C. This is hotter than the hot and thin (1450°C, 95 km) plate GDH1 and, importantly, much hotter than estimates of normal mantle temperature from mid-ocean ridge basalts. The latter indicate a potential temperature T_p of ∼1300°C (T_p = 1280°C [*McKenzie and Bickle*, 1988], T_p = <1395°C [*Kinzler and Grove*, 1992], T_p = 1260°C [*Kojitani and Akaogi*, 1997], which (e.g., via equation (5) [*McKenzie and Bickle*, 1988]) is consistent with a sublithospheric mantle temperature of about 1350°C [*McKenzie*, 1984].

[68] In contrast to the high T_b estimates, our estimates of α at values of ∼2.6 × 10^{-5} °C^{-1} are at the lower end of compiled estimates from ambient conditions 2.5–4.5 × 10^{-5} °C^{-1} [*Doin and Fleitout*, 1996] and lower than previous values of 3.1 × 10^{-5} °C^{-1} and 3.85 × 10^{-5} °C^{-1} used by *Parsons and Sclater* [1977], *Stein and Stein* [1992], and *Doin and Fleitout* [1996].

[69] These differences from previous analyses, especially NPC1 of *Stein and Stein* [1993], may in part be explained by the depths considered to represent the current plate-scale thermal state of the lithosphere. Plates fitted to data that progressively include more bathymetric features (e.g., models E–A in Table 3) become progressively thinner, cooler, and more expansive. These values are plotted as solid squares on a solid line in Figures 11d–11f. Model E is hidden under the white star (from earlier) of model D, models C to A plot progressively further away from the star. The final point on the line, however, is model U, which is like A but is forced to have a zero-age depth of 2600 m [*Stein and Stein*, 1992, 1993]. For model U, α is dramatically increased (↑∼0.7 °C^{-1}), T_b lowered (↓∼30°C), and the plate thinned (↓∼6 km) to values very close to those of NPC1 [*Stein and Stein*, 1993] (marked by cross). Other factors, for example, the assumed k, however, also have a large effect.

[70] Starting from model D and varying k (models L–S, solid line with circles on Figures 11d–11f) has a different effect, and an estimate closer to that of *Parsons and Sclater* [1977] is possible. Interestingly, this proximity is not entirely arbitrary. Closer estimates occur when basal temperature, T_b, is constrained by crustal thickness, c, and L, α,

and k are all inverted for (i.e. also constrained). T_b is constrained at about 1360°C by the c values of *White* [1992] (7.1 ± 0.8 km) using the geochemical relations of *McKenzie* [1984] or *White and McKenzie* [1995], to give models J and K, respectively. These are shown as diamonds on Figures 11d–11f. The misfit criterion, s^2, now used is

$$s^2 = \frac{1}{n}\sum\frac{(z_{\text{model}} - z_{\text{data}})^2}{\sigma_z^2} + \frac{1}{m}\sum\frac{(q_{\text{model}} - q_{\text{data}})^2}{\sigma_q^2} + \frac{(c_{\text{model}} - c_{\text{data}})^2}{\sigma_c^2} \quad (7)$$

where c_{data} and σ_c^2 are from *White et al.* [1992] and c_{model} is from the geochemical relations. The values of k required for models J and K are 3.9 W m^{-1} °C^{-1}, which is not unreasonably different from experimental constraints. In ambient condition silicates have a thermal conductivity of 4.5–5.5 W m^{-1} °C^{-1}, which reduces to 2.7 or possibly 2.0 W m^{-1} °C^{-1} at the base of the lithosphere [*Hofmeister*, 1999]. Thus values of k representative of the lithosphere between 3 and 4 W m^{-1} °C^{-1} do not appear unreasonable, even when the pressure-temperature dependencies involved are considered [*Doin and Fleitout*, 1996].

[71] Another strong effect on the values of the best fit parameters may come from limits in our understanding of the surface heat flow data. For example, these data may also contain a 4 mW m^{-2} contribution because of radioactive heating in the lithosphere [*Parsons and Sclater*, 1977], which reduces T_b by over 100°C, raises α (model V), and reduces s^2. The misfit reduction should not be over-interpreted, however, as it continues reducing with increasing amounts of q assigned to being radiogenic simply because flatter model q-t curves are possible.

[72] In order to determine if a model less hot and inexpansive can be found, our final model, X (Table 3), combined several patterns observed above and is a four-parameter inversion in which both the crustal thickness constrains the basal temperature and 4 mW m^{-2} of surface heat flow is allowed to be radiogenic. Then T_b = 1363°C, k = 3.371 W m^{-1} °C^{-1}, α = 2.77 ± 0.40 × 10^{-5} °C^{-1}, and L = 120 km, all within experimental constraints although α remains a little low. Thus, being the most physically reasonable, these are our preferred parameters for the conventional plate model. We caution, however, against the literal use of these parameters, especially without consideration first being given to a physical mechanism for the plate model.

[73] In section 1, we assert a dichotomy of scales. Specifically, that hot spot swells, which may have formed by thermal rejuvenation of the lithosphere, are distinct from and superimposed on a "plate-scale" thermal behavior of the lithosphere. However, sublithospheric radiogenic heating and small-scale convection are argued to be a dynamically viable mechanism for providing heat at the base of a cooling plate [*Huang and Zhong*, 2005]. This raises the possibility that the mechanism supplying heat to the base of a plate and hot spots are related, with the hot spot just the larger-scale end-member manifestation of a size spectrum of mantle convection. If this is so, all sizes and ages of thermal perturbation should be retained as part of the plate-scale trend. In this case, the effect of compositional buoyancy within the lithosphere (i.e., surface volcanism, magmatic underplating, and the buoyant depleted residuum of melting [*Johnson and Carlson*, 1992]) should be isolated from the thermal buoyancy, otherwise the thermal subsidence will be incorrectly estimated. This is clearly difficult to do at the present time.

[74] Future work, we believe, must combine careful data analysis with model refinements. Bathymetry data, we suggest, should be analyzed using techniques similar to MiMIC, and inversions for parameters of the plate model should include constraints from surface heat flow, probably crustal thickness and possibly the geoid. With regard to the model, material parameters (i.e., C_p, k, and α) in the plate model are currently representative averages of temperature- and pressure-dependent quantities. Incorporating these dependencies has little effect on observables (i.e., the shape of z-t and q-t curves) for either CHABLIS [*Doin and Fleitout*, 1996] or conventional plates (D. McKenzie, personal communication, 2004). However, some other parameters of conventional plates, at least, are notably affected. For instance, a temperature-dependent plate that best fits the data of *Parsons and Sclater* [1977] is 106 km thick, ∼15% thinner than the model with constant coefficients (D. McKenzie, personal communication, 2004). So, this should also be investigated. Additionally, we suggest that radiogenic heating in the lithosphere may be an important influence on plate parameters.

5.3. Residual Depth Anomalies and Their Correlations

[75] The models above provide a good first-order approximation of the increase in average depth with age of seafloor once small- and medium-scale features identified to be unrelated to the plate-scale thermal structure of the lithosphere have been isolated and removed. In some regions of the seafloor, there remain, however, deviations from the model curves of ∼±0.5 km. We call these deviations "residual depth anomalies," and the correlations between these and other observables gives some, mostly unsurprising, indications of their origin.

[76] Figure 12a shows the residual depth anomalies obtained by subtracting model D from curve iv of the data set of *Smith and Sandwell* [1997]. The purple through to green areas are highs (i.e., shallow), the most significant of which are labeled 1, 2, 3, and 5. Intervening black to red areas are lows, the largest amplitude of which is labeled 4. Also shown as red circles and lines are the hot spots in the North Pacific and their seamount trails, respectively (except Hawaii) [*Koppers et al.*, 2001], which appear to spatially correlate with highs 2, 3, and 5. We note, however, that these non-Hawaiian hot spots may be not be "classic" examples fed by deep mantle plumes [*Clouard and Bonneville*, 2001].

[77] Figure 12b is a map view of vertically averaged s wave velocities at depths between 0 and 125 km, a depth range chosen because it represents the material conductively cooling in the classic plate model of *Parsons and Sclater* [1977] and therefore in some senses represents the lithosphere. Visually, by following similar age, t, seafloor between the 10 and 20 Ma isochrons, positive shallow anomalies 5 and 3 correspond to slower velocity, probably relatively hot, areas. When an age-related trend, approximated by an average over 10 Myr intervals, is

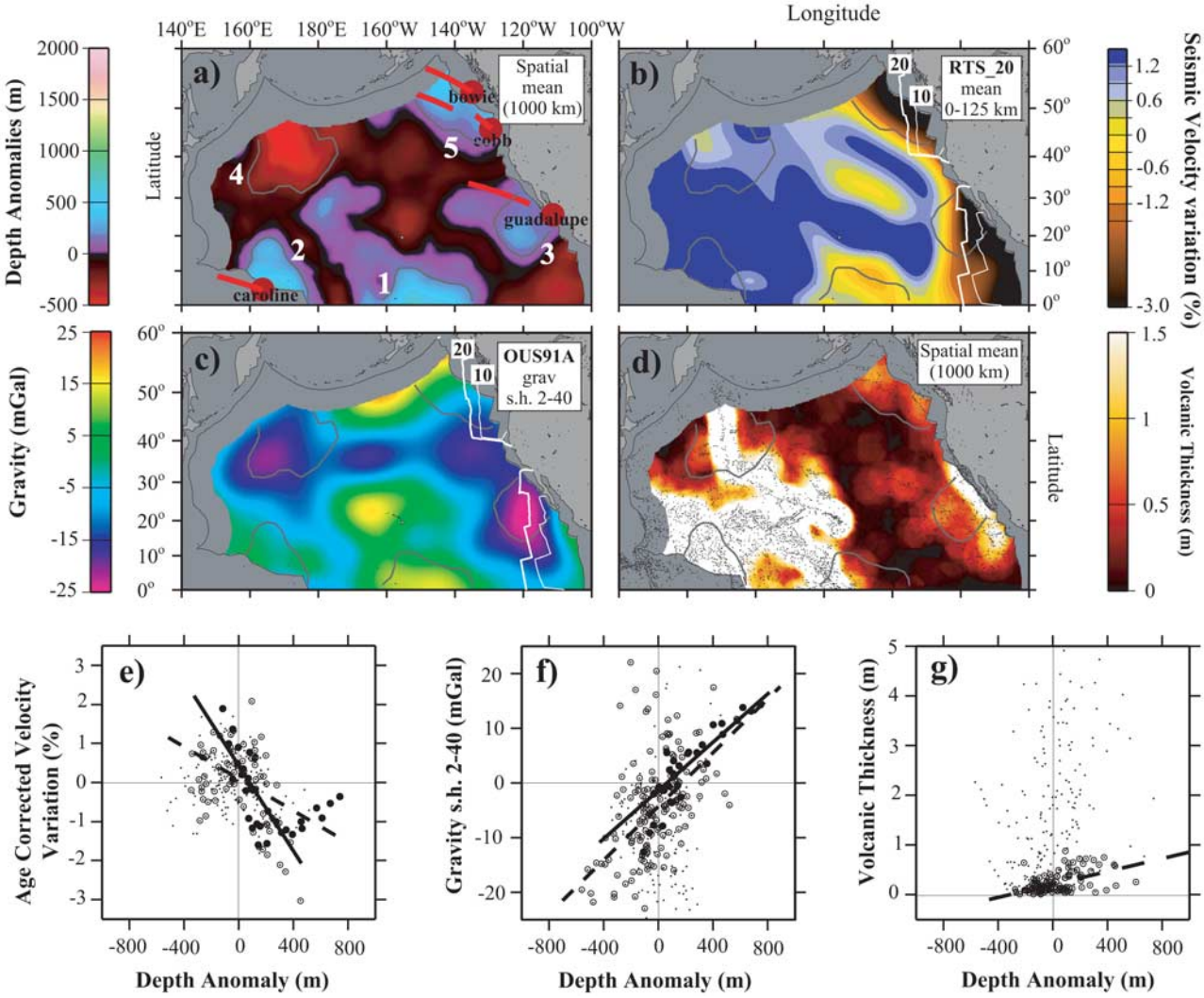

Figure 12. Residual depth anomalies and their correlations with other observables. Depth data set is that of *Smith and Sandwell* [1997]. (a) Depth anomalies, which are deviations of bathymetry after removal of features isolated by two applications of MiMIC from the best fitting plate model (see Figure 10). Anomalies smoothed by 1000 km spatial mean (i.e., grdfilter [*Wessel and Smith*, 1998]). Approximate boundaries of anomalies are gray lines, positive anomalies (i.e., shallow highs) are numbered 1–3 and 5, and negative anomaly is 4. Hot spots (red circles) and associated 0–43 Ma seamount trails (except Hawaii), thick red lines, from *Koppers et al.* [2001, Figure 1] are also shown. (b) Vertically averaged "lithospheric" (i.e., 0–125 km) *S* wave velocity variations from RTS_20 [*Ritsema et al.*, 1999], which has claimed resolution of $\lambda \simeq 2000$ km. Gray lines are depth anomaly boundaries from a), white lines are isochrons (Ma) [Müller and Roest, 1997]. (c) Gravity of spherical harmonics of degree in order 2–40 ($\sim \lambda < 1000$ km) of OUS91a [*Rapp and Pavlis*, 1990]. Boundaries are same as Figure 12a; isochrons are the same as Figure 12b. (d) Volumes of volcanic edifices estimated from satellite altimetry [*Wessel and Lyons*, 1997] smoothed as Figure 12a. Boundaries are same as Figure 12a. (e) Correlation between depth anomalies and lithospheric velocity variations after trend related to seafloor age (mean in 10 Myr intervals) has been removed. Data are resampled at $4° \times 4°$ by grdsample [*Wessel and Smith*, 1998]. Points are all data, circled points are from <40 Ma seafloor and best fitted by the dashed trend line (-2.1% km^{-1}). Black circles are from the region of positive anomaly 1 east of the Line Islands (155°W < longitude < 130°W, 0°N < latitude < 16°N) and the main trend of these anomalies <400 m fitted by the solid trend (-5.5% km^{-1}). As uncertainties are present in both data sets, trends are fitted by orthogonal distance regression (see Appendix A1) (f) Correlation with gravity. Symbols are same as Figure 12e except circled points for ages >70 Ma, which are fitted by the dashed trend (24.6 mGal km^{-1}). Area east of the Line Islands is fitted by solid trend (22.1 mGal km^{-1}). (g) Volcanic thickness correlation. Symbols are same as Figure 12e except circled points 20–80 Myr, which are best fitted by dashed trend (0.65 m km^{-1}).

removed from these "lithospheric" velocities, the age-corrected velocities and residual depth anomalies correlate weakly (r^2 = 0.1397, where r is the linear correlation coefficient or Pearson's r) if statistically significantly (Spearman rank-order correlation and Student's t test; see, e.g., *Press et al.* [1992]). The correlation, however, is better (r^2 = 0.2069) for t < 40 Ma but, we believe, only good enough to interpret the sense of the trend (dashed on Figure 12e) fitted by "orthogonal distance regression" (see Appendix A1). Giving equal weight to the sublithospheric upper mantle (125–660 km) further increases r^2 from 0.2069 to 0.2772. This, we suggest, indicates contributions to surface topography from both the lithosphere and below.

[78] The gravity field at similar scales to the depth anomalies (Figure 12c) is weakly positively correlated (r^2 = 0.1367), although it strengthens for t > 70 Ma to r^2 = 0.2777. This correlation has a slope of 24.6 mGal km^{-1} and is shown on Figure 12f as a dashed line. A stronger correlation still (r^2 = 0.4760) with a slope of 24.8 mGal km^{-1} is achieved if the area (175°W < longitude <150°W, 16°N < latitude <30°N) is excluded such that the Hawaiian Swell is removed from the gravity as it has been from the bathymetry. We only trust this trend semiquantitatively, but it is consistent with deep direct (mass dipole) compensation. It is not consistent with the type of convective compensation proposed for the South Pacific Superswell that produces a negative gravity-topography correlation [e.g., *McNutt and Judge*, 1990].

[79] Figure 12d shows the erupted volume of seamounts as derived from satellite altimetry using an entirely different method to this paper [*Wessel and Lyons*, 1997]. For 20 < t < 80 Ma this correlates (r^2 = 0.2156, Figure 12g) with residual depth anomalies that no longer contain seamounts. This implies a common cause for the seamounts and the depth anomalies.

[80] The only "strong" correlations with residual depth that we have found are for lithospheric tomography (r^2 = 0.6655) and gravity (r^2 = 0.8001) in the approximate area of anomaly 1 east of the Line Islands (155°W < longitude < 130°W, 0°N < latitude < 16°^{N}), which includes part of the cross lines. These are the solid trend lines in Figures 12e–12f and correspond to slopes of −5.5% km^{-1} and 22.1 mGal km^{-1}. Taking these quantities literally, the tomography requires a lithospheric contribution to surface topography while the gravity implies some deeper (i.e., convective) support.

[81] In summary, insufficient correlation exists to safely claim that all the residual depth anomalies have a single simple explanation, such as being the planform of convection in the fluid mantle [e.g., *McKenzie and Richter*, 1976; *McKenzie et al.*, 1980; *McKenzie*, 1983]. High >20 mGal km^{-1} slopes, however, maintain this as a possibility [see *Watts*, 1976]. Other correlations are open to less ambiguous interpretation. On young seafloor, depth anomalies appear to relate to patterns of seismic velocity, which implies that the depth anomalies result from density differences in the lithosphere and below. The shallow depths are associated with increased seamount volcanism, some of which have been identified as related to hot spots. On older seafloor, specifically east of the Line Islands, correlations can be strong and indicate a deep (from gravity) but significantly lithospheric (from tomography) origin for the topography. Volcanism here, however, appears to be limited, presumably by the thicker lithosphere.

6. Conclusions

[82] We draw the following conclusions from this analysis of bathymetry data in the North Pacific Ocean:

[83] 1. When small-scale (i.e., seamounts and oceanic islands) and medium-scale (i.e., oceanic plateaus and hot spot swells) bathymetric features are removed, North Pacific seafloor depths, z (m), are best approximated by subsidence proportional to the root of crustal age, t (Ma), for ages younger than 85 Ma. Depths then flatten asymptotically to ~6.1 km, about 1 km and greater than 2σ shallower than an extrapolation from young seafloor.

[84] 2. Empirical equations describing the subsidence are $z = 3010 + 307\sqrt{t}$ for $t \leq 85$ *Ma* and $z = 6120 - 3010 \exp(-0.026t)$ for $t > 85$ *Ma*. Mean differences from measurements are 51.0 and 62.1 m, respectively.

[85] 3. Our depth-age curve more closely resembles early more empirical estimates [*Parsons and Sclater*, 1977; *Schroeder*, 1984], which are deeper than estimates based on statistical estimators (i.e., mean, median, and mode), and we postulate that this is because these estimators do not remove all the features unrelated to plate-scale subsidence. This result is robust to the bathymetry data set used and isolated height contour used to define the medium-scale oceanic plateaus, rises, and swells.

[86] 4. There is no abrupt change in the bathymetry that reflects the plate-scale thermal variation of the lithosphere as reported by *Carlson and Johnson* [1994] and *Smith and Sandwell* [1997]. Thus, even if the seafloor is more complex in detail than the model predicts [e.g., *Calcagno and Cazenave*, 1994], a single cooling plate model provides a good first-order approximation to both old and young seafloor simultaneously. In this sense cooling plate models are applicable to oceanic bathymetry.

[87] 5. The best fitting cooling plate model, assuming a thermal conductivity, k, of 3.138 W m^{-2} [*Parsons and Sclater*, 1977; *Stein and Stein*, 1992], has a plate thickness, L, of 115 ± 16 km, basal temperature, T_b, of 1522 ± 180 °C, and coefficient of thermal expansion, α, of 2.57 ± 0.40 × 10^{-5} °C^{-1}. This is unreasonably hot, however, and also very inexpansive.

[88] 6. More reasonable material parameters for the model can be attained by constraining basal temperature by crustal thickness using geochemical relations to ~1350°C and allowing for some (4 mW m^{-2}) surface heat flow to be radiogenic in origin. These are T_b = 1363°C, k = 3.371 W m^{-1} °C^{-1}, α = 2.77 ± 0.40 × 10^{-5} °C^{-1} and L = 120 km, although given the flexibility we have found in determining these parameters we are concerned about their literal interpretation.

[89] 7. We have used the best fit cooling plate model to calculate residual depth anomalies in the North Pacific Ocean. On young, but not old, seafloor shallow areas are associated with seamount volcanism, some of which has previously been assigned to hot spots. At wavelengths of 1000 to several 1000 km the anomalies are ~±500 m in amplitude and appear, from tomography

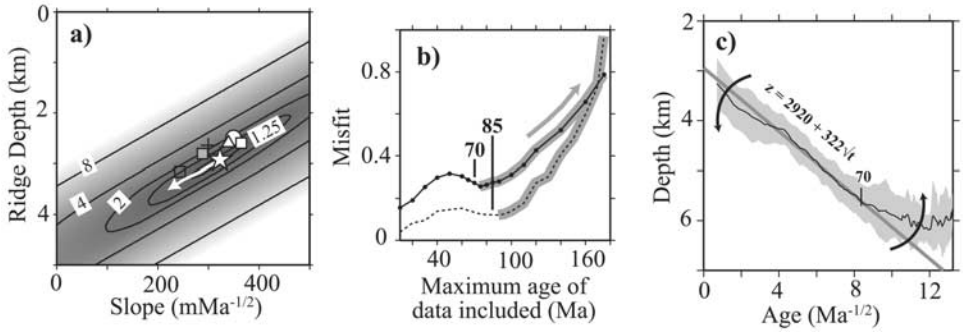

Figure A1. Plot of the square root of time for a different misfit criterion. See Figure 9.

and gravity ($\sim$25 mGal km^{-1}) correlations, to originate both in the lithosphere and below (i.e., by convection). This is especially true to the east of the Line Islands where there are strong correlations. Insufficient correlation exists, however, to claim with any certainty a single, simple origin for all the depth anomalies such as the planform of mantle convection.

Appendix A

A1. Calculation of Geoid to Topography Ratio

[90] The ratio of geoid to topography in the Magellan Rise was calculated to be between 1.08 and 1.50 m km^{-1} (regions 180–174°W, 4–10°N and 180–170°W 0–10°N, respectively). The ratios were computed as did [*Marks and Sandwell*, 1991] except we used no tapering of wavelength amplitude coefficients, and compute the orthogonal distance regression (ODR) [e.g., *Boggs et al.*, 1988] by "brute force" testing of all lines.

[91] Cosine tapering wavelengths between 2000 km and 10,000 km (grdfft [*Wessel and Smith*, 1998]) produces intermediate geoid to topography ratios. The data used here are the OUS91a gravity solution [*Rapp and Pavlis*, 1990] and ship track data from the NGDC database binned in 0.1° × 0.1° areas (i.e., blockmode [*Wessel and Smith*, 1998]) and then gridded with an untensioned bicubic spline (i.e., surface [*Wessel and Smith*, 1998]).

[92] ODR is used because uncertainties are present in both data sets. It minimizes the perpendicular distance between point and line rather than the vertical distance as in ordinary least squares fitting. Orthogonal distance regression is also known as, among other things, as "non-biased linear regression" [*Marks and Sandwell*, 1991, p. 8048], or "generalized least squares estimates" [*Anderson*, 1984, p. 7], and may be made robust [*Brown*, 1982].

A2. Effect of Error Estimator Used in the Fitting Calculations

[93] The half-space and cooling plate fitting calculations in the main text were conducted using s^2, a standard deviation normalized variance, as by *Stein and Stein* [1992]. Worth noting, however, is the uncertainty that results from the choice of misfit estimator used. For example, using

$$s = \frac{1}{n}\sum \frac{|z_{\text{model}} - z_{\text{data}}|}{\sigma_z} + \frac{1}{m}\sum \frac{|q_{\text{model}} - q_{\text{data}}|}{\sigma_q} \qquad \text{(A1)}$$

suggests that the depth-age curve iv of *Smith and Sandwell* [1997] is best described by a square root of time subsidence of $z = 2990 + 322\sqrt{t}$ for $t \leq 70$ Ma (Figure A1). This in turn leaves older seafloor described by $z = 6125 - 4050\exp(-0.029t)$ and alters the best fitting plate parameters ($\uparrow \alpha$, $\downarrow T_b$, L approximately unchanged) to L = 112 km, $\alpha = 2.79 \times 10^{-5}$ °C^{-1} and T_b = 1487°C (model W).

[94] **Acknowledgments.** We thank Katie Johnston and members of the Marine Lab, Alistair Crosby for contributions based on his masters thesis, and Dan McKenzie for code relating crustal thickness and asthenospheric temperature. We are grateful to Pål Wessel, Richard Carlson, and an anonymous Associate Editor for their constructive reviews and Dan McKenzie for his comments. The GMT software of Pål Wessel and Walter Smith was widely used in both computations and figures. This work was supported by a NERC studentship to J.H. and a NERC/ROPA award to A.B.W. Additional support for J.H. provided by Derrick and Muriel Davey, thank you.

References

Abrams, L. J., R. L. Larson, T. H. Shipley, and Y. Lancelot (1993), Cretaceous volcanic sequences and Jurassic oceanic crust in the East Marianas Basin of the western Pacific, in *The Mesozoic Pacific: Geology, Tectonics and Volcanism*, *Geophys. Monogr. Ser.*, vol. 77, edited by M. S. Pringle et al., pp. 77–101, AGU, Washington, D. C.

Anderson, T. W. (1984), Estimating linear statistical relationships, *Ann. Stat.*, *12*(1), 1–45.

Boggs, P. T., C. H. Spiegelman, J. R. Donaldson, and R. B. Schnabel (1988), A computational examination of orthogonal distance regression, *J. Econ.*, *38*, 169–201.

Brown, M. L. (1982), Robust line estimation with errors in both variables, *J. Am. Stat. Assoc.*, *77*, 71–79.

Buck, W. R. (2001), Accretional curvature of lithosphere at magmatic spreading centres and the flexural support of axial highs, *J. Geophys. Res.*, *106*, 3953–3960.

Calcagno, P., and A. Cazenave (1994), Subsidence of the sea-floor in the Atlantic and Pacific oceans—Regional and large-scale variations, *Earth Planet. Sci. Lett.*, *126*, 473–492.

Carlson, R. L., and H. P. Johnson (1994), On modeling the thermal evolution of the oceanic upper mantle: An assessment of the cooling plate model, *J. Geophys. Res.*, *99*, 3201–3214.

Castillo, P. R., R. W. Carlson, and R. Batiza (1991), Origin of the Nauru Basin igneous complex: Sr and Nd and Pb isotope and REE constraints, *Earth Planet. Sci. Lett.*, *103*, 200–213.

Castillo, P. R., P. A. Floyd, and C. France-Lanord (1992), Isotope geochemistry of leg 129 basalts: Implications for the origin of the widespread cretaceous volcanic event in the Pacific, *Proc. Ocean Drill. Program Sci. Results*, *129*, 405–412.

Cazenave, A., S. Houry, B. Lago, and K. Dominh (1992), Geosat-derived geoid anomalies at medium wavelength, *J. Geophys. Res.*, *97*, 7081–7096.

Clouard, V., and A. Bonneville (2001), How many Pacific hot-spots are fed by deep-mantle plumes?, *Geology*, *29*, 695–698.

Colin, P., and L. Fleitout (1990), Topography of the ocean floor: Thermal evolution of the lithosphere and interaction of deep mantle heterogeneities with the lithosphere, *Geophys. Res. Lett.*, *17*, 1961–1964.

Crough, T. S. (1978), Thermal origin of mid-plate hot-spot swells, *Geophys. J. R. Astron. Soc.*, *55*, 451–469.

Crough, T. S. (1979), Hotspot epirogeny, *Tectonophysics*, *61*, 321–333.
Crough, T. S. (1983), The correction for sediment loading on the seafloor, *J. Geophys. Res.*, *88*, 6449–6454.
Davies, G. F., and F. Pribac (1993), Mesozoic seafloor subsidence and the Darwin Rise, past and present, in *The Mesozoic Pacific: Geology, Tectonics and Volcanism*, *Geophys. Monogr. Ser.*, vol. 77, edited by M. S. Pringle et al., pp. 39–52, AGU, Washington, D. C.
Davis, A. S., M. S. Pringle, L. B. G. Pickthorn, D. A. Clague, and W. C. Shawab (1989), Petrology and age of alkalic lava from the Ratak chain of the Marshall Islands, *J. Geophys. Res.*, *94*, 5757–5774.
Davis, A. S., L. B. Gray, D. A. Clague, and J. R. Hein (2002), The Line Islands revisited: New $^{40}Ar/^{39}Ar$ geochronologic evidence for episodes of volcanism due to lithospheric extension, *Geochem. Geophys. Geosyst.*, *3*(3), 1018, doi:10.1029/2001GC000190.
Davis, E. E., and C. R. B. Lister (1974), Fundamentals of ridge crest topography, *Earth Planet. Sci. Lett.*, *21*, 405–413.
Den, N., et al. (1969), Seismic-refraction measurements in the northwest Pacific Basin, *J. Geophys. Res.*, *74*, 1421–1435.
Detrick, R. S., and S. T. Crough (1978), Island subsidence, hot-spots and lithospheric thinning, *J. Geophys. Res.*, *83*, 1236–1244.
Doin, M. P., and L. Fleitout (1996), Thermal evolution of the oceanic lithosphere: An alternative view, *Earth Planet. Sci. Lett.*, *142*, 121–136.
Ewing, J., M. Ewing, T. Aitken, and W. J. Ludwig (1968), North Pacific sediment layers measured by seismic profiling, in *The Crust and Upper Mantle of the Pacific Area*, *Geophys. Monogr. Ser.*, vol. 12, edited by L. Knopoff, C. L. Drake, and P. J. Hart, pp. 147–173, AGU, Washington, D. C.
Floyd, P. A., and P. R. Castillo (1992), Geochemistry and petrogenesis of Jurassic ocean crust basalts, Site 801, *Proc. Ocean Drill. Program Sci. Results*, *129*, 361–385.
Gettrust, J. F., K. Furukawa, and L. W. Kroenke (1980), Crustal structure of the Shatsky Rise from seismic refraction measurements, *J. Geophys. Res.*, *85*, 5411–5415.
Haggerty, J. A., S. O. Schlanger, and I. P. Silva (1982), Late Cretaceous and Eocene volcanism in the southern Line Islands and implications for hotspot theory, *Geology*, *10*, 433–437.
Harland, W. B., R. L. Armstrong, A. V. Cox, L. E. Craig, A. G. Smith, and D. G. Smith (1990), *A Geologic Timescale 1989*, Cambridge Univ. Press, New York.
Haxby, W. F., and J. K. Weissel (1986), Evidence for small-scale mantle convection from Seasat altimeter data, *J. Geophys. Res.*, *91*, 3507–3517.
Heestand, R. L., and T. S. Crough (1981), The effect of hot spots on the oceanic age-depth relation, *J. Geophys. Res.*, *86*, 6107–6114.
Heezen, B. C., J. L. Matthews, R. Catalano, J. Natland, A. Coogan, M. Tharp, and M. Rawson (1973), Western Pacific guyots, *Initial Rep. Deep Sea Drill. Proj.*, *20*, 653–700.
Heezen, R. P., M. J. Cordery, R. S. Detrick, and C. Fang (1989), Heat-flow and thermal origin of hot-spot swells: The Hawaiian Swell revisited, *J. Geophys. Res.*, *94*, 13,783–13,799.
Hillier, J. K., and A. B. Watts (2004), "Plate-like" subsidence of the East Pacific Rise-South Pacific Superswell system, *J. Geophys. Res.*, *109*, B10102, doi:10.1029/2004JB003041.
Hofmeister, A. M. (1999), Mantle values of thermal conductivity and geotherm from phonon lifetimes, *Science*, *283*, 1699–1705.
Houtz, R. E., and W. J. Ludwig (1979), Distribution of reverberant subbottom layers in the southwest Pacific Basin, *J. Geophys. Res.*, *84*, 3497–3504.
Huang, J., and S. Zhong (2005), Sublithospheric small-scale convection and its implications for the residual topography at old ocean basins and the plate model, *J. Geophys. Res*, doi:10.1029/2004JB003153, in press.
Humler, E., C. Langmuir, and V. Daux (1999), Depth vs age: New perspectives from the chemical compositions of ancient crust, *Earth Planet. Sci. Lett.*, *173*, 7–23.
Intergovernmental Oceanographic Commission (IOC) (2003), GEBCO 1-minute grid [CD-ROM], UNESCO, Paris. (available at http://www.ngdc.noaa.gov/mgg/gebco/)
Jackson, E. D., and S. O. Schlanger (1976), Regional syntheses, Line Islands chain, Tuamotu Island chain, and Manihiki Plateau, central Pacific Ocean, *Initial Rep. Deep Sea Drill. Proj.*, *33*, 915–927.
Jarvis, G. T., and W. R. Peltier (1980), Oceanic bathymetry profiles flattened by radiogenic heating in a convecting mantle, *Nature*, *285*, 649–651.
Johnson, P. H., and R. L. Carlson (1992), Variations of sea floor depth with age: A test of models based on drilling results, *Geophys. Res. Lett.*, *19*, 1971–1974.
Johnson, R. H. (1971), Reduction of discrepancies at crossing points in geophysical surveys, *J. Geophys. Res.*, *76*, 4892–4896.
Jordan, T. H. (1979), Mineralogies, densities and seismic velocities of garnet lherzolites and their geophysical implications, in *The Mantle Sample: Inclusions in Kimberlites and Other Volcanics*, edited by F. R. Boyd and H. O. A. Meyer, pp. 1–14, AGU, Washington, D. C.
Kane, K. A., and D. E. Hayes (1992), Tectonic corridors in the South Atlantic: Evidence for long-lived mid-ocean ridge segmentation, *J. Geophys. Res.*, *97*, 17,317–17,330.
Kinzler, R. J., and T. L. Grove (1992), Primary magmas of mid-ocean ridge basalts: 2. Applications, *J. Geophys. Res.*, *97*, 6907–6926.
Kojitani, H., and M. Akaogi (1997), Melting enthalpies of mantle peridotite: Calorimetric determinations in the system CaO-MgO-Al_2O_3-SiO_2 and applicaition to magma generation, *Earth Planet. Sci. Lett.*, *153*, 209–222.
Koppers, A. A. P., J. P. Morgan, J. W. Morgan, and H. Staudigel (2001), Testing the fixed hotspot hypothesis using $^{40}Ar/^{39}Ar$ age progressions along seamount trails, *Earth Planet. Sci. Lett.*, *185*, 237–252.
Kulp, J. L. (1963), Potassium-argon dating of volcanic rocks, *Bull. Volcanol.*, *26*, 247–258.
Lancelot, Y., et al. (1990), Old Pacific crust, *Proc. Ocean Drill. Program Initial Rep.*, *129*, 33–83, 91–161, 171–237.
Langseth, M. G., X. Le-Pichon, and M. Ewing (1966), Crustal structure of mid-ocean ridges, *J. Geophys. Res.*, *71*, 5321–5351.
Larson, R. L. (1991), Latest pulse of Earth: Evidence for a mid-Cretaceous superplume, *Geology*, *19*, 547–550.
Ludwig, W. J., and R. E. Houtz (1979), Isopach map of the sediments in the Pacific Ocean Basin and marginal seas basins, *AAPG Map Ser. 647*, Am. Assoc. of Pet. Geol., Tulsa, Okla.
Madsen, J. A., D. W. Forsyth, and R. S. Detrick (1984), A new isostatic model for the East Pacific Rise crest, *J. Geophys. Res.*, *89*, 9997–10,015.
Malinverno, A. (1990), A quantative study of the axial topography of the Mid-Atlantic Ridge, *J. Geophys. Res.*, *95*, 2645–2660.
Marks, K. M., and D. T. Sandwell (1991), Analysis of geoid height versus topography for oceanic plateaus and swells using nonbiased linear regression, *J. Geophys. Res.*, *96*, 8045–8055.
Marty, J. C., and A. Cazenave (1989), Regional variations in subsidence rate of oceanic plates: A global analysis, *Earth Planet. Sci. Lett.*, *94*, 301–315.
Matthews, J. L., B. C. Heezen, R. Catalano, A. Coogan, M. Tharp, J. Natland, and M. Rawson (1974), Cretaceous drowning of reefs on Mid-Pacific and Japanese guyots, *Science*, *184*, 462–464.
McAdoo, D. C., and D. T. Sandwell (1989), On the source of cross-grain lineations in the central Pacific gravity field, *J. Geophys. Res.*, *94*, 9341–9352.
McKenzie, D. (1984), The generation and compaction of partially molten rock, *J. Petrol.*, *25*, 713–763.
McKenzie, D., and M. Bickle (1988), The volume of melt generated by extension of the lithosphere, *J. Petrol.*, *29*, 625–679.
McKenzie, D. P. (1967), Some remarks on heat flow and gravity anomalies, *J. Geophys. Res.*, *72*, 6261–6273.
McKenzie, D. P. (1983), The Earth's mantle, *Sci. Am.*, *249*(3), 67–80.
McKenzie, D. P., and F. Richter (1976), Convection currents in the Earth's mantle, *Sci. Am.*, *235*(5), 72–89.
McKenzie, D. P., A. B. Watts, B. Parsons, and M. Roufosse (1980), Planform of mantle convection beneath the Pacific Ocean, *Nature*, *288*, 442–446.
McNutt, M., and A. V. Judge (1990), The superswell and mantle dynamics beneath the South Pacific, *Science*, *248*, 969–975.
McNutt, M. K. (1995), Marine geodynamics: Depth-age revisited, *U.S. Natl. Rep. Int. Union Geod. Geophys. 1991–1994, Rev. Geophys.*, *33*, 413–418.
McNutt, M. K., and K. M. Fischer (1987), The South Pacific Superswell, in *Seamounts, Islands and Atolls*, *Geophys. Monogr. Ser.*, vol. 43, edited by B. H. Keating et al., pp. 25–34, AGU, Washington, D. C.
McNutt, M. K., E. L. Winterer, W. W. Sager, J. H. Natland, and G. Ito (1990), The Darwin Rise: A Cretaceous superswell?, *Geophys. Res. Lett.*, *17*, 1101–1104.
Menard, H. (1956), Archipelagic aprons, *Am. Assoc. Pet. Geol. Bull.*, *40*, 2195–2210.
Menard, H. W. (1969), Elevation and subsidence of oceanic crust, *Earth Planet. Sci. Lett.*, *6*, 275–284.
Menard, H. W., and S. M. Smith (1966), Hypsometry of ocean basin provinces, *J. Geophys. Res.*, *71*, 4305–4325.
Moore, W. B., and G. Schubert (1997), Lithospheric thinning and chemical buoyancy beneath the Hawaiian Swell, *Geophys. Res. Lett.*, *24*(11), 1287–1290.
Morgan, J. P., and W. H. F. Smith (1992), Flattening of the seafloor depth-age curve as a response to asthenospheric flow, *Nature*, *359*, 524–527.
Morgan, W. (1971), Convection plumes in the lower mantle, *Nature*, *230*, 42–43.

Müller, R. D., and W. R. Roest (1997), Digital isochrons of the world's ocean floor, *J. Geophys. Res.*, *102*, 3211–3214.
Nagihara, S., C. R. B. Lister, and J. G. Sclater (1996), Reheating of old oceanic lithosphere: Deductions from observations, *Earth Planet. Sci. Lett.*, *139*, 91–104.
Nakanishi, M., W. W. Sager, and A. Klaus (1999), Magnetic lineations within Shatsky Rise, northwest Pacific Ocean: Implications for hot spot–triple junction interaction and oceanic plateau formations, *J. Geophys. Res.*, *104*, 7539–7556.
National Geophysics Data Center (NGDC) (2003a), GEODAS version 4.1, http://www.ngdc.noaa.gov/mgg/gdas/g4_sys.Html.
National Geophysics Data Center (NGDC) (2003b), Total sediment thickness of the world's oceans and marginal seas, http://www.ngdc.noaa.gov/mgg/sedthick/sedthick.html.
National Oceanic and Atmospheric Administration (NOAA) (1988), Data announcement 88-MGG-02, digital relief of the surface of the Earth, Natl. Geophys. Data Cent., Boulder, Colo.
O'Connell, R. J., and B. H. Hager (1980), On the thermal state of the Earth, in *Physics of the Earth's Interior*, edited by A. Dziewonski and E. Boschi, pp. 270–317, Elsevier, New York.
Parsons, B., and D. McKenzie (1978), Mantle convection and the thermal structure of the plates, *J. Geophys. Res.*, *83*, 4485–4496.
Parsons, B., and J. Sclater (1977), An analysis of the variation of ocean floor bathymetry and heat flow with age, *J. Geophys. Res.*, *82*, 803–827.
Phipps Morgan, J., E. M. Parmentier, and J. Lin (1987), Mechanisms for the origin of mid-ocean ridge axial topography: Implications for the thermal and mechanical structure of accreting plate boundaries, *J. Geophys. Res.*, *92*, 12,823–12,836.
Phipps Morgan, J., W. J. Morgan, and E. Price (1995), Hotspot melting generates both hotspot volcanism and a hotspot swell, *J. Geophys. Res.*, *100*, 8045–8062.
Pollack, H. N., S. J. Hunter, and J. R. Johnson (1993), Heat flow from the Earth's interior: Analysis of the global data set, *Rev. Geophys.*, *31*, 267–280.
Press, W. H., S. A. Teukolsky, W. T. Vetterling, and B. P. Flannery (1992), *Numerical Recipies in FORTRAN 77: The Art of Scientific Computing, FORTRAN Numer. Recipies*, vol. 1, 634 pp., Cambridge Univ. Press, New York.
Pringle, M. S. (1992), Radiometric ages of basaltic basement recovered at Sites 800, 801, and 802, leg 129, western Pacific Ocean, *Proc. Ocean Drill. Program Sci. Results*, *129*, 389–399.
Rapp, R. H., and N. K. Pavlis (1990), The development and analysis of geopotential coefficient models to spherical harmonic degree 360, *J. Geophys. Res.*, *95*, 21,885–21,911.
Rea, D. K., and T. L. Vallier (1983), Two Cretaceous volcanic episodes in the western Pacific Ocean, *Geol. Soc. Am. Bull.*, *94*, 1430–1437.
Renkin, M. L., and J. G. Sclater (1988), Depth and age in the North Pacific, *J. Geophys. Res.*, *93*, 2919–2935.
Ritsema, J., H. J. van Heijst, and J. H. Woodhouse (1999), Complex shear wave velocity structure imaged beneath Africa and Iceland, *Science*, *286*, 1925–1928.
Sager, W. W., and H.-C. Han (1993), Rapid formation of the Shatsky Rise oceanic plateau inferred from its magnetic anomaly, *Nature*, *364*, 610–613.
Sager, W. W., and B. H. Keating (1984), Paleomagnetism of Line Islands seamounts: Evidence for late Cretaceous and early Tertiary volcanism, *J. Geophys. Res.*, *89*, 1135–1151.
Sager, W. W., J. Kim, A. Klaus, M. Nakanishi, and L. M. Khankishieva (1999), Bathymetry of the Shatsky Rise, northwest Pacific Ocean: Implications for oceanic plateau development at a triple junction, *J. Geophys. Res.*, *104*, 7557–7576.
Sandwell, D. T., and K. R. MacKenzie (1989), Geoid height versus topography for oceanic plateaus and swells, *J. Geophys. Res.*, *94*, 7403–7418.
Sandwell, D. T., and M. Renkin (1988), Compensation of swells plateaus in the North Pacific: No direct evidence for mantle convection, *J. Geophys. Res.*, *93*, 2775–2783.
Schlanger, S. O., H. C. Jenkyns, and I. Premolisilva (1981), Volcanism and vertical tectonics in the Pacific Basin related to global Cretaceous transgressions, *Earth Planet. Sci. Lett.*, *52*, 435–449.
Schlanger, S. O., M. O. Garcia, B. H. Keating, J. J. Naughton, W. W. Sager, J. A. Haggerty, J. A. Philpots, and R. A. Duncan (1984), Geology and geochronology of the Line Islands, *J. Geophys. Res.*, *89*, 1261–1272.
Schroeder, W. (1984), The empirical age-depth relation and depth anomalies in the Pacific Ocean, *J. Geophys. Res.*, *89*, 9873–9883.
Schubert, G., and D. Sandwell (1989), Crustal volumes of the continents and of oceanic and continental submarine plateaus, *Earth Planet. Sci. Lett.*, *92*, 234–246.
Schubert, G., and D. L. Turcotte (1972), One-dimensional model of shallow-mantle convection, *J. Geophys. Res.*, *77*, 945–951.
Schubert, G., D. A. Yuen, C. Froidevaux, L. Fleitout, and M. Souriau (1978), Mantle circulation with partial shallow return flow: Effects on stresses in oceanic plates and topography of the seafloor, *J. Geophys. Res.*, *83*, 745–758.
Sclater, J. G., R. N. Anderson, and L. M. Bell (1971), Elevation of ridges and evolution of the central eastern pacific, *J. Geophys. Res.*, *76*, 7888–7915.
Shipley, T. H., J. M. Whitman, F. K. Duennebier, and L. D. Petersen (1983), Seismic stratigraphy and sedimentation history of the East Marianas Basin, western Pacific, *Earth Planet. Sci. Lett.*, *64*, 257–275.
Shipley, T. H., L. J. Abrams, Y. Lancelot, and R. L. Larson (1993), Late Jurassic - early Cretaceous oceanic crust and early Cretaceous volcanic sequences of the Nauru Basin, western Pacific, in *The Mesozoic Pacific: Geology, Tectonics and Volcanism*, *Geophys. Monogr. Ser.*, vol. 77, edited by M. S. Pringle et al., pp. 103–119, AGU, Washington, D. C.
Sichoix, L., A. Bonneville, and M. K. McNutt (1998), The seafloor swells and superswell in French Polynesia, *J. Geophys. Res.*, *103*, 27,123–27,133.
Sleep, N. H., and S. Biehler (1970), Topography and tectonics at the intersection of fracture zones and central rifts, *J. Geophys. Res.*, *75*, 2748–2752.
Smith, W. (1993), On the accuracy of digital bathymetric data, *J. Geophys. Res.*, *98*, 9591–9603.
Smith, W. H. F. (1990), Marine geophysical studies of seamounts in the Pacific Ocean Basin, Ph.D. thesis, 216 pp., Columbia Univ., New York.
Smith, W. H. F., and D. T. Sandwell (1997), Global sea floor topography from satellite altimetry and ship depth soundings, *Science*, *277*, 1956–1962.
Smith, W. H. F., and P. Wessel (1990), Gridding with continuous curvature splines in tension, *Geophysics*, *55*, 293–305.
Stein, C., and S. Stein (1993), Constraints on Pacific midplate swells from global depth-age and heat flow-age models, in *The Mesozoic Pacific: Geology, Tectonics and Volcanism*, *Geophys. Monogr. Ser.*, vol. 77, edited by M. S. Pringle et al., AGU, Washington, D. C.
Stein, C. A., and S. Stein (1992), A model for the global variations in oceanic depth and heat flow with lithospheric age, *Nature*, *359*, 123–129.
Tamaki, K., and R. L. Larson (1988), The Mesozoic tectonic history of the Magellan microplate in the western central Pacific, *J. Geophys. Res.*, *93*, 2857–2874.
Turcotte, D. L., and G. Schubert (2002), *Geodynamics*, 2nd ed., 456 pp., Cambridge Univ. Press, New York.
Vallier, T. L., W. E. Dean, D. K. Rea, and J. Thiede (1983), Geologic evolution of Hess Rise, central north Pacific Ocean, *Geol. Soc. Am. Bull.*, *94*, 1289–1307.
Van Wykhouse, R. (1973), Synbaps, *Tech. Rep. TR-233*, Natl. Oceanogr. Off., Washington, D.C.
Verzhbitskii, E. V., and L. R. Merklin (2000), Geothermal regime and origin of the Shatsky Rise, *Oceanology*, *40*(4), 583–589.
Vogt, P. R. (1967), Steady state crustal spreading, *Nature*, *215*, 811–817.
Wang, X., and J. Cochran (1993), Gravity anomalies, isostasy, and mantle flow at the East Pacific Rise crest, *J. Geophys. Res.*, *98*, 19,505–19,531.
Watts, A. B. (1976), Gravity and bathymetry in the central Pacific Ocean, *J. Geophys. Res.*, pp. 1533–1548.
Watts, A. B. (2001), *Isostasy and Flexure of the Lithosphere*, 458 pp., Cambridge Univ. Press, New York.
Watts, A. B., J. H. Bodine, and N. M. Ribe (1980), Obsevations of flexure and the geological evolution of the Pacific Ocean Basin, *Nature*, *283*, 532–537.
Watts, A. B., D. P. McKenzie, B. E. Parsons, and M. Roufosse (1985), The relationship between gravity and bathymetry in the Pacific Ocean, *Geophys. J. R. Astron. Soc.*, *83*, 263–298.
Wessel, P. (1989), XOVER—A crossover error detector for track data, *Comput. Geosci.*, *15*, 333–346.
Wessel, P. (1998), An empirical method for optimal robust regional-residual separation of geophysical data, *Math. Geol.*, *30*, 391–408.
Wessel, P., and S. Lyons (1997), Distribution of large Pacific seamounts from Geosat/ERS-1, *J. Geophys. Res.*, *102*, 22,459–22,475.
Wessel, P., and W. H. F. Smith (1998), New, improved version of Generic Mapping Tools released, *Eos Trans. AGU*, *79*, 579.
Wessel, P., and A. B. Watts (1988), On the accuracy of marine gravity measurements, *J. Geophys. Res.*, *93*, 393–413.
Wessel, P., L. W. Kroneke, and D. Bercovici (1996), Pacific plate motion and undulations in the geoid and bathymetry, *Earth Planet. Sci. Lett.*, *140*, 53–66.
White, R. S., and D. McKenzie (1995), Mantle plumes and flood basalts, *J. Geophys. Res.*, *100*, 17,543–17,585.

White, R. S., D. McKenzie, and R. K. O'Nions (1992), Oceanic crustal thickness from seismic measurements and rare-earth-element inversions, *J. Geophys. Res.*, *97*, 19,683–19,715.

Windom, K. E., K. E. Seifert, and T. L. Vallier (1981), Igneous evolution of Hess Rise: Petrological evidence from DSDP leg 62, *J. Geophys. Res.*, *86*, 6311–6322.

Winterer, E. L., and C. V. Metzler (1984), Origin and subsidence of guyots in Mid-Pacific Mountains, *J. Geophys. Res.*, *89*, 9969–9979.

Winterer, E. L., J. I. Ewing, R. G. Douglas, R. D. Jarrard, Y. Lancelot, R. M. Moberly, T. C. Moore, P. H. Roth, and S. O. Schlanger (1973), Leg 17: Honolulu to Hawaii, *Initial Rep. Deep Sea Drill. Proj.*, *17*, 146, 913.

Wolfe, C. J., and M. K. McNutt (1991), Compensation of Cretaceous seamounts of the Darwin Rise, northwest Pacific Ocean, *J. Geophys. Res.*, *96*, 2363–2374.

Wood, B. J., and D. A. Yuen (1983), The role of lithospheric phase transitions on seafloor flattening at old ages, *Earth Planet. Sci. Lett.*, *66*, 303–314.

J. K. Hillier and A. B. Watts, Department of Earth Science, University of Oxford, Parks Road, Oxford, OX1 3PR, UK. (johnh@earth.ox.ac.uk; tony@earth.ox.ac.uk)